博士論文

Humanization and characterization of anti-epiregulin monoclonal antibody

(抗エピレギュリンモノクロナール抗体の
ヒト型化と機能評価)

氏　名　　李　泳薫　(Lee Young-Hun)

Abstract

The epidermal growth factor (EGF) signaling system consists of at least seven ligands, namely, EGF, amphiregulin, transforming growth factor α, heparin-binding EGF, betacellulin, epiregulin (EREG), and epigen (Yarden and Sliwkowski, 2001). These ligands bind to the extracellular region of the epidermal growth factor receptor (EGFR) and induce a conformational change, leading to receptor dimerization and activation. Activated EGFR stimulates a variety of intracellular signaling pathways, including the mitogen-activated protein kinase pathway and the phosphoinositide 3-kinase/Akt pathway, leading to cell proliferation, cell survival, and angiogenesis (Yarden and Sliwkowski, 2001; Fischer et al., 2003). In tumors, the EGFR ligands are produced by either the malignant cells themselves or the surrounding stromal cells, causing constitutive activation of EGFR (Salomon et al., 1995). Of the EGFR ligands, EREG is produced as a transmembrane precursor that exerts a mitogenic effect on various cell types, including hepatocytes and human cancer cells, in particular, on epithelial tumor cells (Toyoda et al., 1995). EREG is expressed at relatively low levels in most adult tissues and its expression has been found to be high in many human cancers, including those of the colon, breast, prostate, and ovary (Baba et al., 2000; Freimann et al., 2004; Tørring et al., 2005; Revillion et al., 2007). A number of studies have examined the involvement of EREG in tumorigenesis and showed the oncogenic effects of its overexpression. Because of its involvement in the oncogenesis, EREG has been considered as a therapeutic target. To this end, several anti-EREG murine monoclonal antibodies (mAbs) have been generated to successfully detect tumor cells in transplanted mouse models

with high sensitivity (unpublished data). However, one of the primary problems in developing monoclonal antibodies as clinical drugs is the human anti-mouse antibody response (HAMA), which limits the administration of murine antibodies to humans (Carter, 2001). When humanizing the therapeutic murine anti-EREG antibody, the key issue is to preserve their affinity without losing the biological activity. The purpose of this study was to reduce the immunogenicity of the murine 9E5 monoclonal antibody through antibody humanization, while maintaining acceptable binding activity.

In this report, I describe the design, construction, and expression of humanized anti-EREG antibody accomplished by variable domain resurfacing studies performed on the basis of the computer-aided three-dimensional (3D) structure of the variable domain fragment (Fv) of a murine anti-EREG monoclonal antibody. Initially, human consensus sequence was used as a template to design the amino acid sequence of the variable region of humanized antibody. However, the initial version of humanized antibody (HM0) was shown to have significantly lower antigen-binding affinity. Grafting the CDRs of murine antibodies onto appropriate human frameworks has often resulted in lower affinity or specificity for the target antigen. There are some general strategies for the recovering the binding affinity of humanized antibodies prepared by the CDR grafting method. These strategies often require several trial-and-error approaches (Gram et al., 1992). In this study, a reliable 3D model of the variable regions of the 9E5 antibody was built by computer-aided homology modeling. This molecular model suggested that the residue 49 in the light chain variable region (VL) underlying CDR was critical for antigen binding. The back mutation L49Y (tyrosine to histidine) generated the humanized version HM1, which produced an antibody that had binding ability similar to that of its murine counterpart.

Importantly, mutation of one amino acid in the framework was sufficient to recover the binding capacity of a humanized antibody. Additionally, the heavy and light chain frameworks of HM1 showed a humanness score (Abhinandan and Martin, 2007) of 0.270 (heavy) and 0.092 (light), respectively, suggesting that the immunogenicity of the humanized anti-EREG antibodies was much lower than that of the original murine antibody. The reduced immunogenicity and enhanced capacity to bind to cancer cells may aid the application of the humanized anti-EREG antibody HM1 in clinical settings.

This study also supports the idea that HM1 contains a human IgG1 constant region that is effective in recruiting human immune system effector function, including complement-dependent cytotoxicity (CDC) and antibody-dependent cellular cytotoxicity (ADCC). All these results show that the humanized anti-EREG antibody is successfully expressed as an IgG1 complete antibody and that this antibody is able to bind specifically to human colorectal carcinoma cells. The humanized anti-EREG antibody has the potential for further development as a candidate therapeutic antibody.

Table of Contents

Abbreviations

4-(*2-hydroxyethyl)-1-piperazineethanesulfonic* acid (HEPES)

Antibody-Dependent Cell-Mediated Cytotoxicity (ADCC)

Antibody-Dependent Cellular Phagocytosis (ADCP)

Antigen binding region (Fab)

Association constant (K_a)

Basic fibroblast growth factor (bFGF)

Chinese hamster ovary (CHO)

Complement-Dependent Cytotoxicity (CDC)

Complementarity-determining region (CDR)

Cytomegalovirus (CMV)

Dalton (Da)

Dissociation constant (K_d)

Endoplasmic reticulum (ER)

Epidermal Growth Factor (EGF)

Epidermal growth factor receptor (EGFR)

Epiregulin (EREG)

Ethylene glycol tetraacetic acid (EGTA)

Ethylenediaminetetraacetic acid (EDTA)

Fc-gamma receptors (FcγR)

Fetal bovine serum (FBS)

Fragment crystallizable region (Fc region)

Framework region (FR)

G-protein coupled receptors (GPCR)

Heavy and light variable region (VH and VL)

Heparing-binding EGF (HB-EGF)

Human Anti-Chimeric Antibody (HACA)

Human Anti-Mouse Antibodies (HAMA)

Hydrochloric acid (HCl)

Immunoglobulin (Ig)

Master cell banks (MCB)

Mean fluorescent intensity (MFI)

Mitogen- activated protein kinase (MAPK)

Monoclonal antibodies (mAb)

Multiple cloning sites (MCS)

N-[3-(Dimethylamino)propyl]-*N*'-ethylcarbodiimide (EDC)

N-Hydroxysuccinimide (NHS)

Nuclear factor of activated T-cells (NFAT)

Phenylmethanesulfonylfluoride (PMSF)

Phosphate buffered saline (PBS)

Phosphatidylinositol 3` kinase B (PI3K)

Polyacrylamide gel electrophoresis (PAGE)

Polymerase Chain Reaction (PCR)

Protein Data Bank (PDB)

Room temperature (RT)

Roswell Park Memorial Institute medium (RPMI)

Sodium chloride (NaCl)

Sodium dodecyl sulfate (SDS)

Standard errors (S.E.)

Surface plasmon resonance (SPR)

Transforming growth factor α (TGF-α)

Tyrosine kinase inhibitors (TKIs)

Variable fragment (Fv)

Vascular endothelial growth factor (VEGF)

List of Figures

List of Tables

Chapter 1 Introduction

1. 1 Epidermal Growth Factor (EGF)

Intercellular interactions mediated by polypeptide growth factors regulate key biological processes, including embryonic development, neuronal functions, hematopoiesis, and wound healing as well as malignant transformation. Binding of the growth factor induces conformational changes in the receptor, leading to receptor dimerization and activation that frequently unmasks the receptor-intrinsic tyrosine kinase activity (Geer et al., 1994). These receptors fall into several subgroups that exhibit structural and functional similarities. Each subgroup of receptors specifically recognizes a family of structurally homologous growth factors. Perhaps, the most striking multiplicity of related growth factors is exemplified by the epidermal growth factor (EGF) family of molecules (Salomon et al., 1995).

1. 1. 1 EGF family

The EGF family of growth factors consists of a set of ligands that bind to one or more of the four ErbB family receptors. These ligands are divided into three groups. The first group consist of epidermal growth factor (EGF) (Cohen, 1962), transforming growth factor α (TGF-α) (Marquardt et al., 1984), and amphiregulin (Shoyab et al., 1989). Members of this group bind specifically to epidermal growth factor receptor (EGFR) (Carpenter and Cohen, 1990). The second group consist of betacellulin (Hanahan et al., 1993), heparin-binding EGF (HB-EGF)

(Higashiyama et al., 1991), and epiregulin (EREG) (Toyoda et al., 1995). Members of this group bind to both EGFR and HER4/erb-B4. The third group consists of heregulin (neuregulin-1) (Wen et al., 1992), of which neuregulin-1 (Holmes et al., 1992) and neuregulin-2 bind to HER3/erb-B3 and erb-B4, whereas neuregulin-3 and neuregulin-4 bind only to HER4/erb-B4 (Holbro, 2003) (Figure 1. 1).

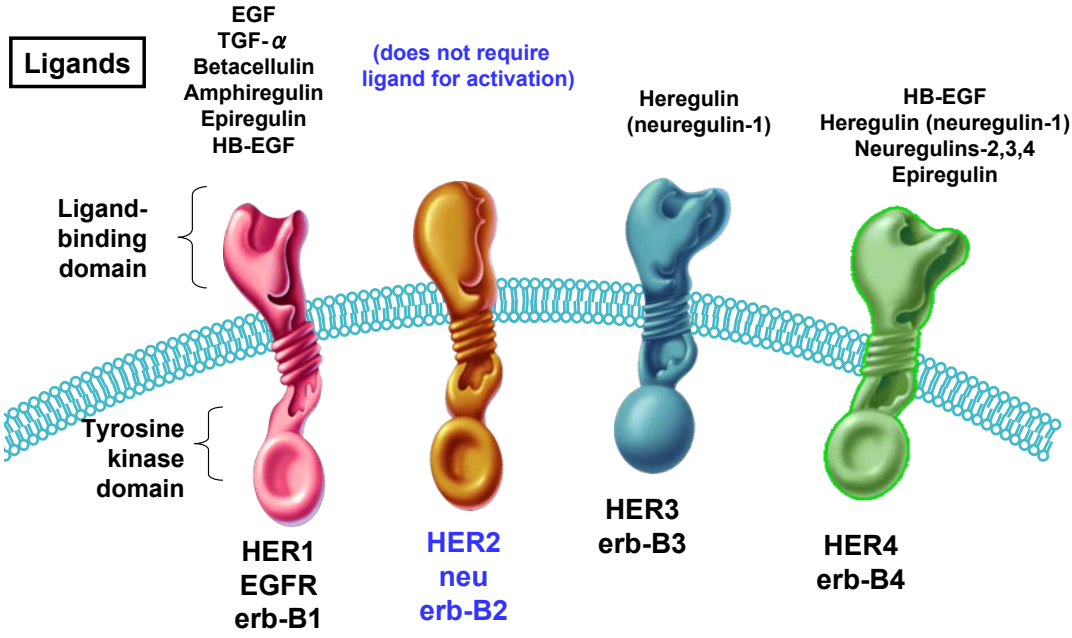

Figure 1. 1. The EGF family and ErbB family receptors. The receptor consists of three domains: a ligand-binding extracellular domain, a transmembrane domain, and an intracellular domain containing a tyrosine kinase region. (EGF, epidermal growth factor; EGFR, EGF receptor; HER, human epidermal receptor; HB-EGF, heparin-binding EGF; NRG, neuregulin; TGF-α, transforming growth factor-α). Adapted from (Rowinsky, 2004).

1. 1. 2 Biochemical and structural characterization of EGF

All EGF family members show a 50–60-amino acid-long sequence and a molecular weight of approximately 6 kDa. The structure of EGF consists of three loops (A-C), connected

by three internal disulfide bonds (Figure 1. 2) (Lu, 2001): Cys1-Cys3, Cys2-Cys4, and Cys5-Cys6, which constitute a consensus sequence that is common to all mature EGFs. Starting from the N-terminus of EGF, the A-loop (amino acid residues 6–19) contains ridges and the B-loop (residues 20–31) is formed by a two-stranded antiparallel β sheet. A part of the second antiparallel β sheet forms the C-loop (residues 32–42) (Ogiso et al., 2002).

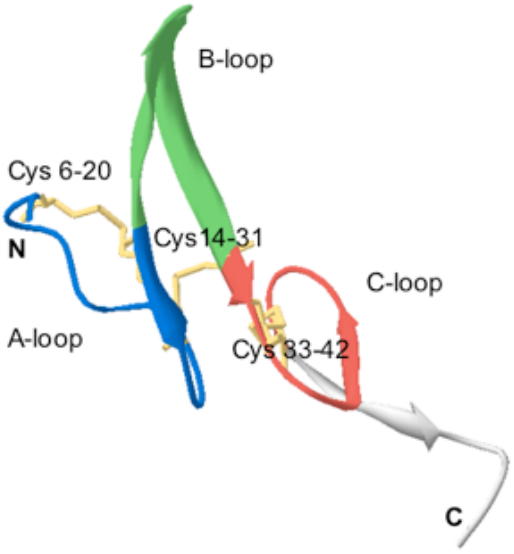

Figure 1. 2. Ribbon model of EGF (PDB-code: 1IVO:D). The A-, B-, and C-loops are colored blue, green and red, respectively. Disulfide bridges are colored yellow.

The biological activities of EGF depend on its binding to a specific receptor, through which it exerts a potent mitogenic effect on majority of epithelial cells, fibroblasts, and endothelial cells (Bennett and Schultz, 1993). EGF-receptor interaction triggers a complex set of downstream biochemical processes that eventually lead to cell cycle progression (Pusztai et al., 1993), and that, to some extent, mirrors the biochemical features of transformed cells (Tannock and Rotin, 1989).

1. 1. 3 EGFR signaling pathway

The EGF family of growth factors is produced as precursors that are integrated into the plasma membrane as type I transmembrane proteins. Mature EGFs are released upon cleavage of the precursor proteins by specific metalloproteinases, which can be activated by G-protein coupled receptors (GPCR) (Daub et al., 1996). In normal cells, under physiologic conditions, the activation of ErbB receptors is controlled by the temporal and spatial expression of their ligands. However, in tumors, ErbB family ligands are produced by either the tumor cell itself or the surrounding stromal cells, leading to constitutive activation of ErbB receptors (Hynes and Lane, 2005). Activated ErbB dimers generate cellular responses by initiating intracellular signaling pathways. Increasing knowledge has transformed the image of the ErbB network from a simple linear pathway into a complex multilayered network, tightly regulated by positive and negative feedback (Ciardiello and Tortora, 2008; Avraham and Yarden, 2011; Okines et al., 2011) (Figure 1. 3).

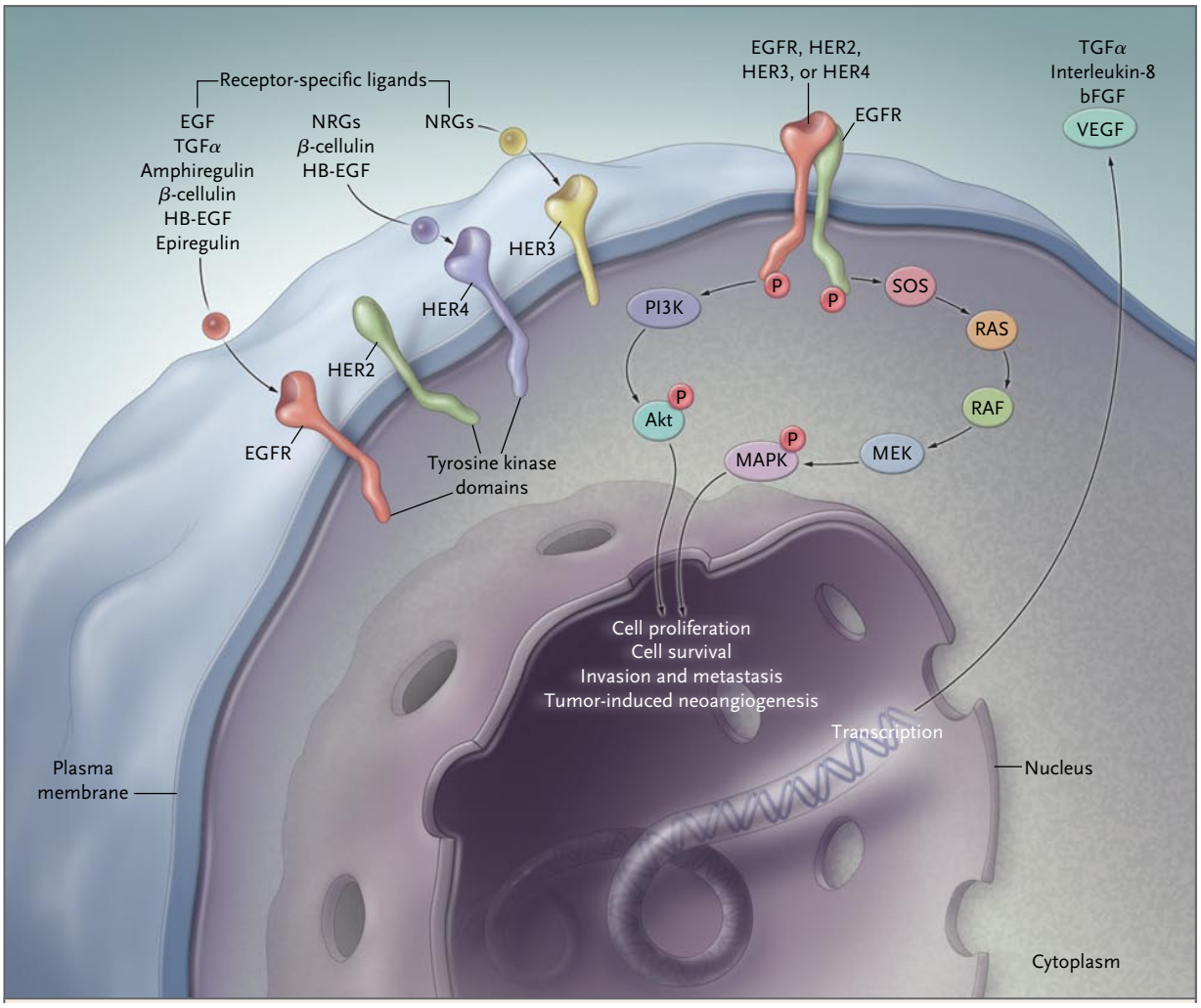

Figure 1. 3. Signal transduction pathways controlled by activation of EGFR. Ligand binding to EGFR results in a conformational change of the receptor, exposing the dimerization domain, and allowing for homodimerization with a second EGFR or heterodimerization with another member of the HER family. Dimerization is essential for receptor function and precedes transactivation of the tyrosine kinase portion via receptor transphosphorylation. The transphosphorylated receptor activates downstream proteins and initiates a signaling cascade, including activation of the Ras/Raf/MAPK pathway, PI3K/AKT, and initiation of gene transcription. Copyright: (Ciardiello and Tortora, 2008).

Two major intracellular pathways are the RAS-RAF-MEK-MAPK pathway and the PI3K-Akt pathway. ErbB-dependent intracellular signaling causes transcriptional activation of specific genes, which induce cell proliferation, inhibit apoptosis, and stimulate invasion,

metastasis, and tumor-induced angiogenesis. Basic fibroblast growth factor (bFGF) and vascular endothelial growth factor (VEGF) are also important players (Ciardiello and Tortora, 2008).

1. 2 EGF and Cancer

1. 2. 1 Role of EGF in cancer development

Clinical studies have shown that overexpression of one or more ligands correlates with decreased patient survival. For instance, expression of TGF-α in colorectal tumors is associated with a >50-fold increase in the risk for liver metastasis (Barozzi et al., 2002). Elevated expression of many ligands in bladder cancer patients is linked to decreased patient survival (Thøgersen et al., 2001). Increased expression of TGF-α in head and neck tumors is correlated with decreased survival (Grandis et al., 1998). Expression of some ligands in tumor cells is associated with resistance to chemotherapeutic drugs (Wang et al., 2007). Despite these observations, the currently approved drugs for cancer treatment that are driven by the ErbB family members target the receptors rather than the ligands. These drugs include monoclonal anti-receptor antibodies and tyrosine kinase inhibitors (TKIs) (Britten, 2004). Acquisition of resistance to chemotherapeutic drugs is often associated with up-regulation of ligands (Valabrega et al., 2005) or other receptors (Engelman et al., 2007), and limits the efficacy of anti-EGFR drugs. Human breast cancer cells selected *in vivo* for resistance to trastuzumab have been found to overexpress EGFR and EGFR ligands (Ritter et al., 2007). Because of drug resistance and moderate clinical efficacies of anti-receptor antibodies and TKIs, alternative therapeutic strategies are required to increase the mean survival rate of patients. For example, a fraction of colorectal and other tumors respond to bevacizumab, an antibody that binds the vascular

endothelial growth factor (Hurwitz et al., 2004). Thus, the multiplicity of EGF-like ligands, along with extensive receptor-receptor interactions, is a potential impediment to similar application of anti-ligand antibodies.

1. 2. 2 Epiregulin (EREG) and molecular targeting of EREG in cancer

Of the EGF family members, EREG was first isolated from the conditioned medium of the mouse tumor cell line NIH3T3/clone T7. EREG does not bind heparin (Toyoda et al., 1995). EREG is located on chromosome 4q13.3 and spans 4.8 kb of DNA (Toyoda et al., 1997). The molecular weight of the mature protein, as revealed by radiolabeling studies, is 5 kDa, representing 46 amino acid residues (Toyoda et al., 1995; 1997). The amino acid sequence of EREG is 24–50% identical to that of other EGF family members.

Compared to other EGF family members, EREG is unique in that it is expressed at low levels in normal adult tissues, whereas its expression is high in various human cancers, including those of the colon, breast, prostate, and ovary (Baba et al., 2000; Freimann et al., 2004; Tørring et al., 2005; Revillion et al., 2007). Many studies have suggested the involvement of EREG in tumorigenesis and the oncogenic effects of high-level cancer-specific expression of EREG. Therefore, EREG is involved in the development of several types of human cancers and it has been intensely pursued as a potential therapeutic target.

1. 3 Therapeutic Antibodies and Antibody Engineering

1. 3. 1 Antibody application in cancer therapy

Research and development of monoclonal antibodies is a rapidly progressing field (Aggarwal, 2007) with >30 antibodies or antibody derivatives approved for human therapy over the past 25 years (Reichert, 2010). Because of target specificity, low toxicity, and ability to activate the immune system, antibodies continue to be considered promising therapeutic agents.

The concept of using serum antibodies for therapeutic targeting of human disease was first proposed by Ehrlich. In 1948, Pressman and Keigley demonstrated antibody localization in the target organ, and in 1952, Beierwalts showed that antibodies labeled with iodine-131 exerted anti-cancer effects in patients (Abrams, 1993). However, the use of antibodies was limited because the antiserum produced was a heterogeneous mixture of antibodies that lacked specificity. In 1975, Kohler and Milstein (Nobel Prize winners, 1984) discovered hybridoma techniques for continuously producing monoclonal antibodies of predefined specificity, a breakthrough in cancer therapy and antibody-based diagnostics. Using hybridoma techniques, many monoclonal antibodies exhibiting anti-cancer activities have been produced by immunizing mice with tumor-associated antigens or intact cancer cells. The spleen cells from immunized mice are isolated and fused with immortalized myeloma cells. Successfully fused hybridoma cells are then screened for the production of a highly specific antibody with anti-cancer activity. Because the interaction between an antibody and its antigen is highly specific, a cancer-specific antibody is able to distinguish cancer cells from normal cells. Cancer-specific antibodies can be used for both cancer imaging and therapy.

1. 3. 2 Antibody structure

Immunoglobulin (Ig) molecules are composed of two types of protein chains: heavy chains and light chains. Furthermore, two types of light chain, termed lambda (λ) and kappa (κ), are found; they do not differ in their functions. Based on the sequence of their heavy chain constant regions, antibodies are divided into five classes: IgM, IgD, IgG, IgE, and IgA. They differ in their biological properties. The functional locations of immunoglobulins and their ability to deal with different antigens are summarized in Table 1. 1.

Table 1. 1. The structural and functional properties of the human immunoglobulin isotypes

Name	Types	Description	Antibody complexes	Half-life in serum
IgA	α1, α2	Mucosal areas, saliva, tears and breast milk; alternative pathway of complement activation; binding to macrophage and phagocyte Fc receptors	Dimer (390 kDa)	6 days
IgD		Antigen receptor on B cells; activates basophils and mast cells	Monomer (184 kDa)	3 days
IgE		Binds to allergens; triggers histamine release from mast cells and basophils; protects against parasitic worms; binding to macrophage and phagocyte Fc receptors	Monomer (188 kDa)	2 days
IgG	γ1, γ2, γ3, γ4	Provides the majority of antibody mediated-based immunity; FcRn mediated placental transport; classical complement activation (not γ4); binding to macrophage and phagocyte Fc receptors (not γ2)	Monomer (146 kDa; γ3: 165 kDa)	21, 20, 7, 21 days
IgM		Expressed on the surface of B cells and in secreted form with very high avidity; eliminates pathogens in the early humoral immunity, CDC	Pentamer (970 kDa)	10 days

Among the various antibodies, IgG is the most commonly used species for therapeutic purposes (Reichert et al., 2005). IgG molecules are ~150-kDa tetramers composed of two identical heavy and light chains linked by disulfide bonds. Antibodies can be divided into two distinct functional units—the fragment of antigen binding (Fab) and the constant fragment Fc (fragment crystallizable; hinge and constant domains CH2 and CH3) (Figure 1. 4).

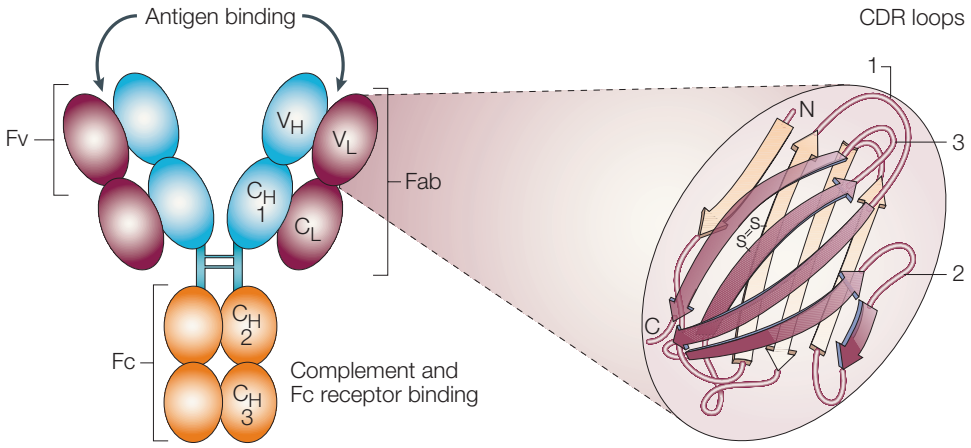

Figure 1. 4. The modular structure of immunoglobulins. This figure shows a single immunoglobulin (Ig) molecule. All immunoglobulin monomers are composed of two identical light (L) chains and two identical heavy (H) chains. Light chains are composed of one constant domain (CL) and one variable domain (VL), whereas heavy chains are composed of three constant domains (CH1, CH2 and CH3) and one variable domain (VH). The heavy chains are covalently linked in the hinge region and the light chains are covalently linked to the heavy chain. The variable domains of both the heavy and light chains compose the antigen-binding, variable domains termed Fv. Within the variable domains there are three loops designated complementarity-determining regions (CDRs) 1, 2, and 3, which confer the highest diversity and define the specificity of antibody binding. Adapted from (Brekke and Sandlie, 2003).

The constant regions of the heavy chains of IgG subclasses show >95% amino acid sequence identity. These constant regions differ primarily in the number of amino acid residues (length) and in the number of interchain disulfide bonds at the hinge region. Both of these features have

an impact on the rotation and flexibility of the IgG and are characteristic of each IgG isotype. Immunoglubulins are also classified by allotype, which reflect the genetic differences within a species. Each IgG has a unique set of physicochemical properties. The human IgG isotypes are summarized in Table 1. 2.

Table 1. 2. Physiochemical properties of human IgG subclasses

	IgG_1	IgG_2	IgG_3	IgG_4
Heavy chain type	gamma 1	gamma 2	gamma 3	gamma 4
Molecular mass (kDa)	146	146	170	146
Amino acids in hinge region	15	12	62	12
Inter-heavy chain disulfide bonds (in hinge region)	2	4	11	2
Susceptibility to proteolytic enzymes	++	+/-	+++	+
Number of allotypes	4	1	13	0

The Fab fragment is composed of one constant and one variable domain of each of the heavy and light chains and contains the variable fragment (Fv), which is responsible for interaction with antigens. The antigen-binding site is formed by six loops, the complementarity-determining regions (CDRs), three of which are present in each of the VH and VL domains. The binding site confers essential properties such as binding affinity and target specificity. The Fc fragment of an antibody is responsible for its immune effector functions and initiates complement-dependent cytotoxicity (CDC), antibody-dependent cellular cytotoxicity (ADCC),

and antibody-dependent cellular phagocytosis (ADCP). Fc also plays a role in controlling the half-life of immunoglobulins through its interactions with the neonatal Fc receptor (FcR).

1. 3. 3 Antibody functions: antibody-dependent cellular cytotoxicity (ADCC)

ADCC, an important mechanism by which antibodies eliminate tumor cells, may propagate the "signal" through the hinge region after binding Fc receptors. Antibodies designed for selective elimination of cancer cells typically require both complement activation and effector-mediated killing via ADCC (Nimmerjahn and Ravetch, 2008).

ADCC is a part of the adaptive immune response, and occurs when effector cells of the immune system, such as macrophages, natural killer cells (NK), and antigen-specific cytotoxic T cells, lyse a target cell bound by specific antibodies. This adaptive immune response depends on a prior antibody response. Cytotoxic T-cells release cytokines in response to antigen binding to antibody Fc receptors located on their cell surface. These cytokines induce apoptosis (cell death) of the target cell. Macrophages and NK cells act to destroy intracellular pathogens. The NK cell also has an Fc receptor, FcγRIII (CD16), on its surface that recognize the Fc portion of antibody bound to the antigen (Nimmerjahn and Ravetch, 2006). The importance of Fc-FcγR interactions for the *in vivo* antitumor effects of therapeutic antibodies has been shown in many studies (Ravetch et al., 2000). Polymorphisms in genes encoding FcγRs are correlated with clinical response to antibodies (Cartron et al., 2002).

1. 3. 4 Limitations of using murine antibody in human cancer therapy

Anti-cancer monoclonal antibodies holds great promise for human cancer therapy. However, monoclonal antibodies of murine origin are immunogenic to humans. The human immune system recognizes a murine antibody as a foreign protein and produces human anti-mouse antibodies (HAMA) that binds the murine antibody, preventing it from reaching its target (Carter, 2001). The HAMA response can also reduce the serum half-life of the murine antibody (Presta et al., 1993), making it therapeutically ineffective. Further, this response may lead to side effects associated with repeated administration of the murine antibody. The immune complex formed between the murine antibody and HAMA can become trapped in the capillary beds of the skin, glomerulus, and other sites, potentially leading to a fatal condition called serum thickness (George, 1994). Therefore, the HAMA responses severely limit the effectiveness of monoclonal antibodies of mouse origin in cancer treatment.

Use of human anti-cancer antibodies will eliminate immunogenicity and HAMA response. However, for various technical reasons, it is very difficult to produce human monoclonal antibodies (George, 1994). An alternative way to prevent HAMA response is to construct an antibody molecule that can evade recognition by the human immune system. This can be done by altering a preexisting murine antibody by genetic engineering to mimic a human antibody. This remodeling process can be accomplished by replacing specific parts of a murine antibody with corresponding parts of a human antibody. This approach is called "antibody humanization".

1. 3. 5 Antibody humanization

The purpose of antibody humanization is to reduce the immunogenicity, while preserving the antigen-binding capacity of the original murine antibody. The simplest approach for this is to produce a chimeric antibody with as few murine parts as possible by replacing the murine constant domains with human constant domains (Figure 1. 5). This chimeric antibody contains fewer murine parts and is less immunogenic to humans than the original murine antibody. However, the murine variable domains of this chimeric antibody are still immunogenic and will trigger a HAMA reaction (Riechmann et al., 1988).

The greater reduction in the immunogenicity of a murine antibody when "humanized" using recombinant DNA technologies allow the production of monoclonal antibodies that possess human features instead of non-essential mouse features (Figure 1. 5).

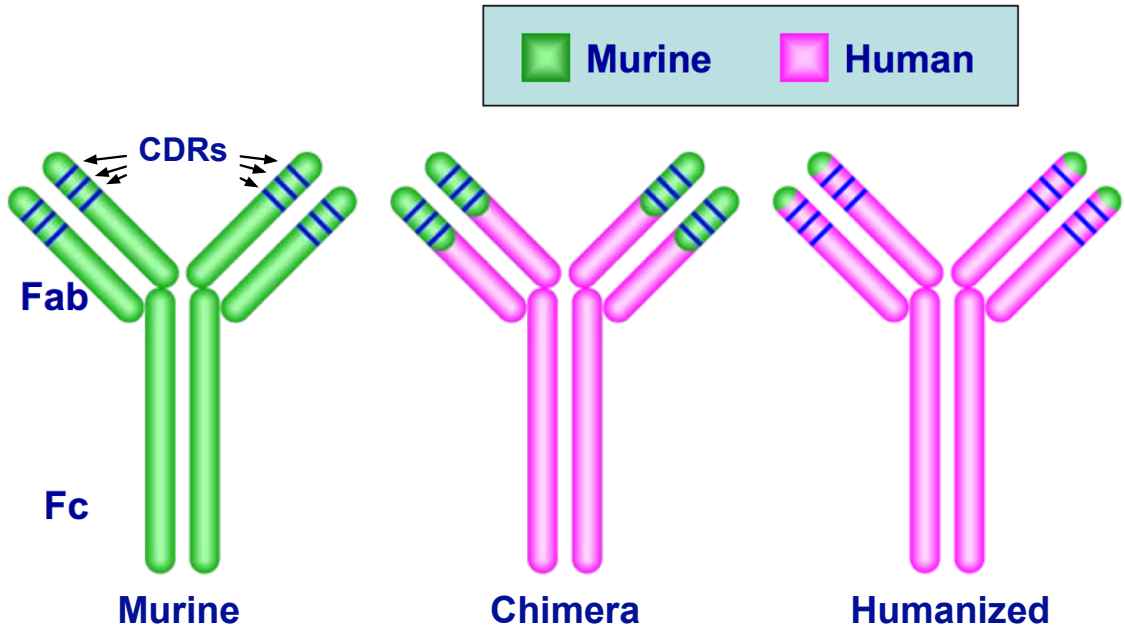

Figure 1. 5. Structure of different antibody humanization products. The structures of different antibody humanization products are shown in the box. The chimeric antibody or antibody fragments contain intact murine variable domains fused to human constant domains without or without the human Fc region. The CDR grafted antibody is produced by grafting only the murine CDRs onto a human antibody. The humanized antibody is composed of a complete human constant region and humanized variable regions.

"Complementarity determining region (CDR)-replacement" (now, better known as CDR-"grafting") was the first described humanization strategy and involves replacing only the CDRs, which constitute the antigen-binding region of an antibody, of a human acceptor antibody with the CDRs of a high-affinity murine antibody (Mian et al., 1991). The sequence of the framework regions of the human acceptor antibody are usually selected based on high homology with the mouse antibody (Jeffrey et al., 1993). In order to retain the original binding capacity, certain framework residues from the original antibody need to be preserved (Padlan, 1994). A process known as “resurfacing”, which involves the replacement of only the solvent-exposed

residues of the folded antibody with the corresponding human sequences, has also been used to humanize antibodies derived from murine sources (Mazor et al., 2007).

To date, a number of humanized antibodies have been constructed for application in cancer therapy. For instance, a humanized murine antibody called CAMPATH-1 has been used to treat patients with lymphoma and appears to have very low immunogenicity (Winter and Harris, 1993).

1. 4 Aim of this study

Several studies have identified the cancer-specific overexpression of EREG is likely involved in tumorigenesis. Therefore, the potential benefit of targeting EREG for cancer treatment is being investigated. To this end, several anti-EREG murine monoclonal antibodies (mAbs) have been generated to sensitively detect tumor cells in transplanted mouse models (unpublished data). A murine mAb, 9E5, was selected from a panel of monoclonal antibodies produced in hybridoma cells by subtractive immunization protocol. Because 9E5 was able to specifically recognize tumor cells with high sensitivity in transplanted mouse models, this antibody is potentially useful for the diagnosis of colon cancer. However, since this monoclonal antibody is of murine origin, it will trigger a HAMA response and is not an ideal candidate for human cancer therapy. One of the challenges faced when humanizing therapeutic murine antibodies is the difficulty in preserving their binding affinity and biological effects simultaneously. The aim of this study was to reduce immunogenicity, while simultaneously maintaining an acceptable level of binding activity of the murine 9E5 monoclonal antibody

through antibody humanization. Development of new anti-EREG antibodies with enhanced effector functions might facilitate their clinical applications.

Chapter 2 Materials and Methods

2. 1 Materials

The anti-EREG antibody 9E5 was a member of a panel of murine monoclonal antibodies (mAbs) generated in hybridoma cells by a subtractive immunization protocol. 9E5, along with its sequence information, was kindly provided as a gift by Dr. Kenji Yoshida (Forerunner Pharma Research, Tokyo, Japan). The coding sequences corresponding to the heavy and light variable regions (VH and VL, respectively) of 9E5, synthesized by Hokkaido System Science (Sapporo, Japan), were inserted into pUC57 vector.

2. 2 Cell Cultures

Human colonic adenocarcinoma cell lines, including HCT116 (American Type Culture Collection [ATCC], CCL-247), DLD-1 (ATCC, CCL-221), and a human gastric cancer cell line, AGS (ATCC, CRL-1739), were a generous gift from Dr. Mariko Iijima (The University of Tokyo, Laboratory for Systems Biology and Medicine). The HCT116 cells were maintained in McCoy's 5A medium (Life Technologies) supplemented with heat-inactivated fetal bovine serum (FBS, Life Technologies) (10%), penicillin (100 IU/mL), and streptomycin (100 IU/mL) (Life Technologies). DLD-1 cells were maintained in RPMI 1646 medium (Life Technologies) containing 10% heat-inactivated FBS, 100 IU/mL penicillin, and 100 IU/mL streptomycin. AGS cells were maintained in RPMI 1646 medium containing 25 mM HEPES, 10% heat-inactivated

FBS, 1% MEM non-essential amino acid solution (Life Technologies), 1 mM sodium pyruvate (Life Technologies), 100 IU/mL penicillin, and 100 IU/mL streptomycin. Typically, 1×10^5 cells were plated onto each 10-cm plate containing 10 mL of the medium and maintained in a humidified atmosphere of 95% air/5% CO_2 at 37°C. Fifty-two hours after plating, the confluent cells were washed twice with PBS, dislodged by trypsinization, resuspended in growth medium, and centrifuged cells at 150 *g* for 5 min. The resulting cell pellet was resuspended in fresh growth medium and seeded on new plates, at a density of 1×10^5 cells.

2. 3 Modeling the Variable Fragment (Fv) of 9E5

2. 3. 1 Antibody structure database for comparative modeling

The 3D structure of the variable region of 9E5 was constructed by homology modeling based on Ig, VH, and VL domains with highly matched amino acid sequence and known structures. Figure 2. 1 illustrates the methodology used for the antibody homology modeling.

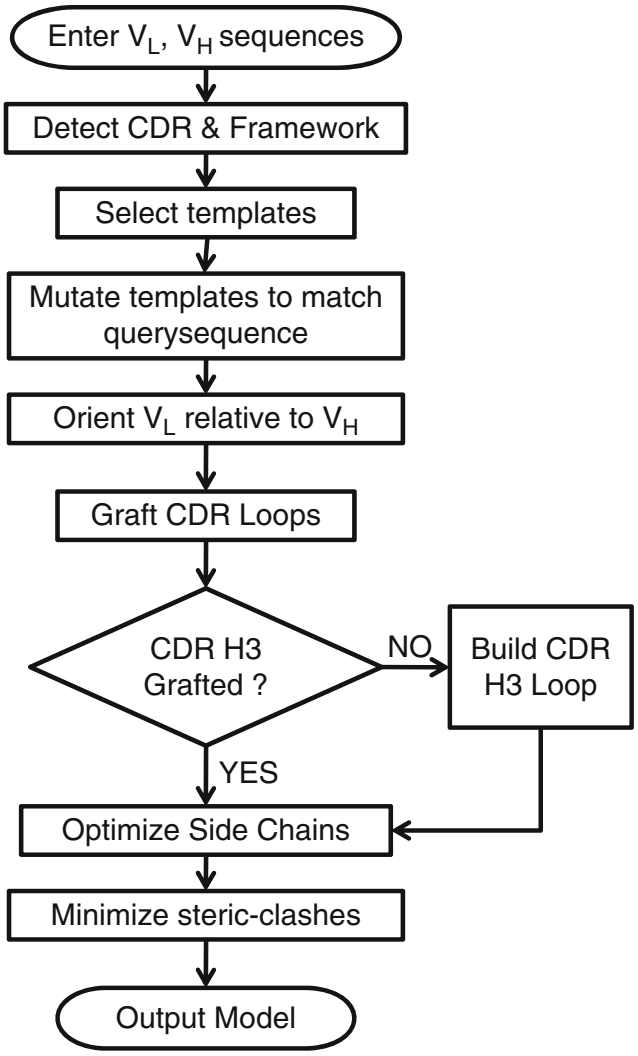

Figure 2. 1. Flowchart illustrating the key steps of antibody homology modeling

First, two separate BLASTP searches were performed for VH and VL. Second, the Protein Data Bank (PDB) was searched for antibody sequences with >70% similarity with the variable region of 9E5 (Allcorn and Martin, 2002). After eliminating NMR structures and crystal structures with resolution above 3.5 Å, a subset of 28 structures were selected. The candidate template structures were selected based on of the IMGT database for residue numbering and the location of the complementarity-determining region (CDR) (Lefranc, 2004). For refining the

models of the CDR, the CDR loop template structures were decided based on the framework region sequence identity of two sides of the CDR loop and the canonical structure type of the CDR loop in the candidate template structures. The canonical structures were used to predict the backbone structures of the CDRs L1-3 and H1-3 (Chothia et al., 1992). The CDR loops H1, H2, and H3 of VH are constituted by residues 27–35, 49–60, and 99–106, respectively, and the CDR loops of VL L1, L2, and L3 are constituted by residues 24–32, 50–56 and 89–96, respectively. Residues outside that defined by CDR constituted the framework regions.

2. 3. 2 CDR H3 modeling

Predicting the CDR H3 is the most challenging part of generating an antibody homology model. The length of CDR H3 varies from 3 to 30 residues and exhibits a great deal of sequence diversity, thus limiting the possibility of capturing the conformation by mere superimpositioning an existing template. In this work, only CDR H3 and the neighboring side chains were remodeled de novo by using a kinematic loop-modeling algorithm in a Rosetta protocol (Sivasubramanian et al., 2009).

Finally, the complex models of the VH and VL of 9E5 were built using RosettaAntibody (Sircar et al., 2009). Two-hundred lowest energy conformations from this run were extracted and subjected to energy minimization. The five lowest energy conformations were used in subsequent analyses. Differences between murine and humanized variants of HM0 antibodies were individually analyzed to investigate their possible influence on the CDRs.

2. 4 Humanization

2. 4. 1 Selection of consensus human frameworks for antibody humanization

I chose human variable regions that are the most homologous in sequence to the murine variable regions as the framework for the humanized 9E5 antibodies. The VH and VL sequences of 9E5 were subjected separately to IgBLAST search against the immunoglobulin Genbank database. A set of data, which contained 1000 human antibody sequences showing highest identities with 9E5, was selected for each variable region, and another set of murine data was chosen in the same way.

2. 4. 2 Humanization of the murine 9E5 variable region

In the humanization process, the murine framework residues potentially influencing the structure of the antigen-binding site were not changed to the corresponding residue of the human framework. Disregarding the CDR residues, several differences were found when comparing the murine selection with the human selection, and these were selected as candidates to be humanized. The candidates from differential residues were selected based on the analysis of the constructed model as well as according to following criteria: (i) the solvent accessible surface area of these candidate structures were computed by CHIMERA (Pettersen et al., 2004); (ii) surface residues of the variable regions of 9E5 (defined as having >30% relative solvent accessibility) (Pedersen et al., 1994) were identified by aligning the sequences of the antibodies of known structure to that of 9E5; (iii) the candidates were differential residues, which could not participate in the formation of intermolecular hydrogen bonds between VH and VL, and intramolecular hydrogen bonds that were important for retaining the conformation of CDRs and

interaction with CDRs directly; and (iv) the candidates were only differential residues but not unique residues.

2. 5 Expression system for humanized 9E5

2. 5. 1 Mammalian cell expression vectors

The IgG expression vector pHMVL-1/pHMVH-1 was constructed by constant region of a human κ light chain (CLIg) and a human IgG1 heavy chain (CHIg) into the vector CET1019-HS-puro (licensed from Millipore). The source of the Ig genes was the plasmid pFUSE-CHIg-hG1/pFUSE2ss-CLIg-hk (InvivoGen) encoding a human monoclonal IgG1 antibody. The first genes encoding human IL2 signal sequence contains 20 amino acids (MYRMQLLSCIALSLALVTNS) which signal peptide of other secretory proteins, was cloned into the multiple cloning sites (MCS). The IgG-encoding genes were amplified by PCR from the pFUSE-CHIg-hG1/pFUSE2ss-CLIg-hk plasmid by using primers (Appendix A1) containing *NheI* restriction sites located on both sides of the open reading frame and that had at least 15 bases of homology with sequences flanking the regions upstream of the human IL2 signal sequence site, for further cloning. The pHM-CLIg/pHM-CHIg plasmid containing the gene encoding signal peptide SS-MCS-VH/VL was considered as an acceptor vector for cloning various genes encoding the IgG of interest into the MCS by using the In-Fusion HD Cloning Kit (Clontech Laboratories, Inc).

HM0/HM1 was amplified from the humanized 9E5 plasmid as a template. The PCR primers designed to join pHM-CLIg/pHM-CHIg, which have 15 base pairs of homology at their

linear ends. The PCR products were cleaved using respective enzymes and agarose gel- purified. Fragments of the correct size, that is, 0.35 kb, were extracted using QIAquick gel elution kit (QIAGEN). The *Nhel*-digested HM0/HM1 fragment was inserted into *Nhel*-digested pHM-CLIg/ pHM-CHIg vector by using the In-Fusion HD Cloning Kit. The mixture containing ligated DNA was transformed into *Escherichia coli* (DH5). The pCET1019-HS-puro vector was likewise digested with respective enzyme and gel purified. To facilitate proper ligation and reduce the background, the cleaved vector was treated with calf intestinal phosphatase (CIP) (Invitrogen). HM0/HM1-LC and HM0/HM1-HC gene fragments were ligated to digested pCET1019-HS-puro vector overnight at room temperature (RT) by using T4 ligase (Invitrogen), thus generating the pHMVL-1 and pHMVH-1 plasmids, respectively. The ligation reactions were used to transform DH5α by heat shock method. Ampicillin-resistant clones were cultured and plasmid DNA was isolated using a mini-prep kit (QIAGEN). Plasmid DNA was linearized and separated by agarose gel electrophoresis to yield fragments of increased size, thus indicating proper insertion of fragment; the desired constructs were confirmed by DNA sequencing.

2. 5. 2 Stable transfections

About 1×10^7 cells of serum-free medium-adapted parent CHO strain (CHO-S cells) were seeded in 125-mL spinner flask and cultured in 30 mL of CHO-S-SFMII medium (Life Technologies) supplemented with 8 mM L-glutamine (Life Technologies). The following day, pHMVL-1 and pHMVH-1 were linearized by *I-SceI* digestion. CHO-S cells were collected by centrifugation from cultures of exponentially growing cells, washed once with PBS, resuspended in PBS at a density of 10^7 cells/mL, and placed on ice. The cells were transfected with a mixture

of 3 μg of pHMVL-1 vector and 2 μg of pHMVH-1 vector (3:2 light chain vector to heavy chain vector) by using AMAXA Nucleofector (Lonza) according to the manufacturer's recommendations. Two days post-transfection, puromycin (Sigma Chemical) was added at a final concentration of 5–15 μg/mL to select stable transfectants. Cells were split 1/2–1/4 once every 3–4 days, and replenished with fresh growth medium containing puromycin. After approximately 2 weeks of selection, the stable cell line was transferred into culture flasks for expansion. Once the cells were recovered (viability > 95%), the antibody expression of the stable cell lines was used to make up the Master cell bank (MCB).

2. 5. 3 Screening of the antibody-producing clones

Serum-free fed-batch culture was carried out in 1-L Erlenmeyer flasks (Corning) at 32°C and 8% CO_2 (v/v) at 125 rpm agitation for 20 days without pH and DO controls. Each clone was inoculated at a density of 5×10^5 cells/mL into serum-free CD FortiCHO™ medium for adaptation, and fed with a 10% v/v serum-free chemically defined feeding medium (CHO CD EfficientFeed A) containing 2 mM L-alanine and 2 mM L-glutamine supplements (all from Life Technologies) on days 4, 7, 11, and 13,. Aliquots of cultures were drawn at days 4, 7, 11, and 13 before adding the feeding medium and at days 15, 18, and 20. Viable cell density was measured with the help of a TC10™ (Bio-RAD) automated cell counter by the Trypan blue exclusion method. The relative viable cell density was calculated by the formula (Figure 2. 2):

100 × (viable cell density) / (maximum viable cell density)

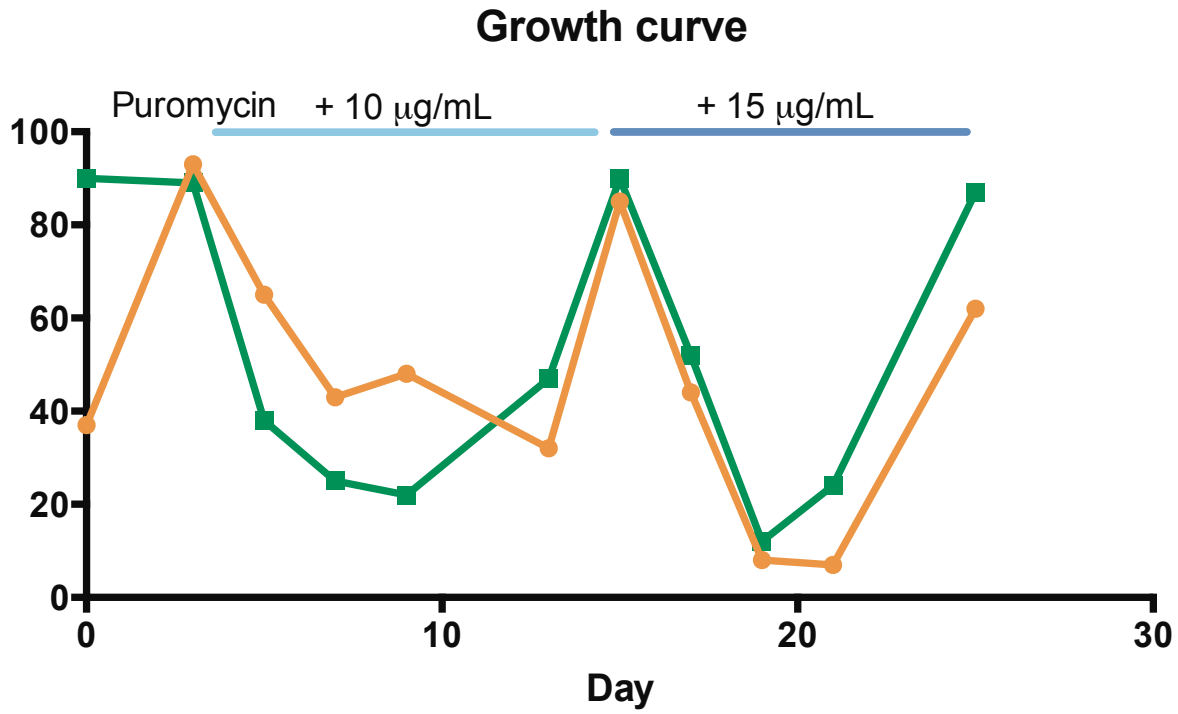

Figure 2. 2. Growth curve of antibody-producing clone Live cell concentration (cells/ml, × 10^4) is shown in orange. Live cells (%) is shown in green.

2. 5. 4 Antibody purification and concentration determination

The cells were incubated for 24 days at 37°C and the supernatant was harvested. Conditioned medium containing human IgG was harvested and filtered through a 0.2-μm filter. The clear supernatant was purified using Bio-Scale™ Mini UNOsphere SUPrA™ (Bio-RAD) according to the manufacturer's recommendations. Eluted antibody was neutralized with 1 M Tris-HCl (pH 9), and the buffer was exchanged through dialysis against PBS overnight. The concentration of the purified antibodies was determined by measuring the absorbance at 280 nm.

2. 6 Characterization of humanized 9E5 antibody

2. 6. 1 Immunoprecipitation

At 80% confluency, HCT116, DLD-1, and AGS cells were collected, washed with cold PBS, and lysed with cold PBS buffer containing 20 mM Tris-HCl (pH 7.5), 150 mM sodium chloride, 1 mM EDTA, 1 mM EGTA, 1% Triton X-100, 2.5 mM sodium pyrophosphate, 1 mM β-glycerolphosphate, 1 mM sodium ortho vanadate, 1 μg/mL leupeptin, 1 mM PMSF, and protease inhibitor cocktail (Roche Diagnostics) and vortexed for 5_min on ice. After 30 min of incubation, the suspensions were centrifuged at 15,000 rpm for 15 min. The cell lysates were stored at −80°C until used. The lysate was used for immunoprecipitation with various antibodies (0.1 μg/mL) and rotated for at least 12 h at 4°C. The mixtures were precleared with Protein A–Sepharose 4FF beads (GE Healthcare) for at least 2 h at 4°C. The suspensions were centrifuged at 4,000 rpm for 1 min. Immunocomplexes were washed with cold lysis buffer three times, resuspended in 2× SDS sample buffer [100 mM Tris-HCl (pH 6.8), 200 mM DTT, 4% SDS, 0.05% bromphenol blue, and 20% glycerol], and subjected to SDS-PAGE and western blot analyses.

2. 6. 2 Western blotting

The precipitated proteins were separated on a 15% SDS polyacrylamide gel. Separated proteins were electro-transferred into a polyvinylidene difluoride membrane (Immobilon-P, Millipore). The membrane was blocked with TTBS [10 mM Tris-HCl (pH 7.5), 0.15 M NaCl, and 0.05% Tween20] containing 1% skim milk for 1 h, followed by incubation with mouse monoclonal antibody to EREG [(Abcam, ab89291), 1:1000] in TTBS containing 1% skim milk for 1 h. After washing with TTBS, the membrane was incubated with HRP-conjugated goat anti-

mouse IgG antibody [(Sigma, A4416), 1:10,000] for 1 h. The membrane was washed with TTBS, and chemiluminescent detection was carried out with the help of Chemi Doc XRS+ (Bio-RAD), according to the manufacturer's instructions.

2. 6. 3 Immunostaining

HCT116, DLD-1, and AGS cells were seeded on 18-mm (circular) coverslips in a 6-well tissue culture dish at 1×10^4 cells/well (5×10^5 cells/mL), and grown as a monolayer at 37°C and 5% CO_2 for 2–3 days. The cells were washed three times, for 5 min each, with phosphate-buffered saline (PBS) containing 0.9 mM $CaCl_2$, 0.33 mM $MgCl_2$ (PBS+) at room temperature (RT). The cells on the coverslips were then fixed with 1 mL of 4% paraformaldehyde/phosphate buffer solution (PFA; WAKO) for 10 min at RT, and permeabilized using either 0.2% Triton X-100 in PBS+ or immediately [non-treatment (-)]. Sections were washed with PBS+ at RT and blocked with PBS+ containing 0.2% fish skin gelatin (PBS/FSG) to eliminate nonspecific staining. Before immunostaining, coverslips were incubated with 1 mL of PBS/FSG for 5 min at RT. After removal of PBS/FSG, the samples were incubated with primary antibodies (9E5, HM0, and HM1) diluted appropriately (0.1 mg/mL) in PBS/FSG (50 μL of diluted primary antibodies were added to each well), and the coverslips were incubated at RT for 1 h. The coverslips were then washed with 2 mL of PBS/FSG three times for 5 min each at RT. Following this, the samples were incubated with secondary antibodies [9E5; Alexa Fluor 488-labeled anti-mouse IgG antibody (Molecular Probes), HM0 and HM1; Alexa Fluor 488-labeled anti-human IgG antibody (Molecular Probes)] diluted appropriately in PBS/FSG (50 μL of diluted secondary antibody was added to each well), at RT for 30 min in dark. The coverslips were then washed

with 2 mL of PBS/FSG three times, for 5 minutes each at RT. Immunostained samples were stained further using Alexa Fluor 594-labeled phalloidin (Molecular Probes), which binds specifically to F-actin. After the removal of the Alexa Fluor 594-labeled phalloidin, the coverslips were washed with 2 mL of PBS+ twice for 5 min each. Following this, samples were washed with 1 mL of sterile H_2O twice for 2 min each. Following the addition of 10 μL of mounting medium (Mobi GLOW mounting medium; Funakoshi), the coverslips were mounted onto slides. Clear nail polish was used to seal the coverslip. Samples were examined using a Leica DM LB fluorescence microscope (Leica Microsystems) equipped with appropriate filters, and photographed with the help of HCX PL APO 60×/1.4 Oil objective or PL APO 100×/1.4 objective operating in the sequential fluorescence image acquisition with 488-nm/FITC or 543-nm/Texas Red excitation lasers and filter set. Fluorescent images were collected using MetaMorph (Molecular Device) software and processed using Adobe Photoshop CS5 (Adobe Systems).

2. 6. 4 Flow cytometry analysis

Cell lines (HCT116, DLD-1, and AGS) were detached from culture plates by treatment with cell dissociation buffer (PBS containing 2 mM EDTA) for 10–20 min at RT and centrifuged at 1000 rpm for 5 min. Cell pellets were washed once with PBS, resuspended in FACS buffer [PBS containing 1% BSA, 0.1 mM EDTA, and 0.01% NaN_3],counted, plated onto 96-well round-bottom tissue culture plate at a density of 1×10^5 cells /well (50 μL/well), and placed on ice for 30 min. After washing three times with ice-cold FACS buffer, cells were incubated in the presence or absence of 0.1, 0.5, and 1 μg/mL antibodies [9E5, HM0, and HM1; antibodies were

labeled with Alexa Fluor 488 by using a monoclonal antibody labeling kit (Molecular Probes)] in 10 μL of ice-cold FACS buffer. After 1-hour incubation on ice in dark, cell were washed three times with ice-cold FACS buffer, resuspended in 200 μL of FACS buffer, and analyzed using FACScan (Guava Express Pro, GE Healthcare). The experiments were performed in triplicate and the data were analyzed with the help of CytoSoft 5.02 (Guava Express Pro, GE Healthcare). The average of mean fluorescent intensity (MFI) of triplicate experiments is presented with standard errors (S.E.).

2. 6. 5 Surface plasmon resonance

Surface plasmon resonance (SPR) measurements were performed using a Biacore™ T200 instrument (GE Health Sciences). Antibodies were immobilized on a CM5 chip by using standard amine-coupling chemistry addressing flow cells individually. This involved activating each flow cell with a freshly mixed solution of 0.2 M EDC in 0.05 M NHS for 5 min and coupling with 3.3 μg/mL antibodies in 10 mM sodium acetate (pH 5.5) for various contact times until 200 RU level was reached. Finally, excess reactive esters were blocked using a 5-min injection of ethanolamine-HCl (GE Health Sciences). One flow cell left unmodified served as a reference surface. Human epiregulin-Fc (MW = 76 kDa), as a ligand for antibodies, were diluted as five-membered fivefold concentration series starting at 1.5 μM, 300 nM, 60 nM, 12 nM, and 2.4 nM into HBS-EP+ buffer [10 mM HEPES (pH 7.4), 150 mM NaCl, 3 mM EDTA, and 0.05% v/v Surfactant P-20, GE Health Sciences]. Each hEpiregulin-Fc was titrated from low- to high-concentration samples. Single-cycle kinetic analysis was performed with an on-time of 120 sec, and an off-time of 600 sec at 30 μL/min. Curve fitting and K_D determinations were performed

with the help of Biacore T200 Evaluation software (GE Health Sciences) and used to evaluate the data, assuming a bivalent analyte model. Thus, the affinity for the direct binding of human epiregulin-Fc over immobilized antibody by SPR was determined following a steady-state approach. The results were based on three independent experiments.

2. 6. 6 ADCC assay

ADCC assays were performed using Jurkat NFAT luciferase reporter cells (Promega), with engineered Jurkat cells stably expressing the FctRIIIa receptor, V158 (high affinity) variant and an NFAT response element driving the expression of firefly luciferase, as effector cells. Target cells (HCT116 and DLD-1, 2×10^4/well) prepared in ADCC assay buffer [RPMI 1640 medium with 4% Low IgG serum (Life Technologies), supplemented with 100 IU/mL penicillin, and 100 IU/mL streptomycin] were added to each round-bottom well of 96-well tissue culture plates. Serial dilutions of antibodies (2,000 ng/mL to 0.3 ng/mL, three-fold dilutions in series) were added to the plates containing the target cells (25 μL/well) and incubated for 2 h at 37°C and 5% CO_2. After washing two times with ADCC assay buffer, Jurkat NFAT luciferase reporter cells (1×10^5/well) were added to each well at a 5:1 effector:target cell ratio, and the plates were incubated further for 24 h. Incubated plates were equilibrated to RT on the bench for 15 min, Bio-Glo™ luciferase assay reagent (Promega) was added to each well, and the plates were incubate at RT for an additional 10 min. Subsequently, the luminescence was measured using a EnSpire Multimode plate reader (PerkinElmer).

Chapter 3 Results

3. 1 Expression profile of EREG in cell lines and tissues

EREG expression in various cell lines and tissues were assessed using an oligonucleotide DNA microarray "GeneChip HG-U133A". Figure 3. 1A & 1B show graphical panels of EREG mRNAs in bar graph format from 112 different human tissues, cultured cells, and cancer cell lines. Gene expression analysis revealed that EREG expression is low in normal tissues and normal cultured cells. In contrast, EREG expression levels varied in cancer cell lines, including colorectal cancer cell lines (DLD-1, Caco-2, HCT116, and LOVO) and gastric cancer cell lines (AGS, KatoIII, MKN45, and MKN74), but in general, not by cancer cell lines. Particularly, elevated expression of EREG was found in colorectal cancer cell lines. In contrast, expression of EREG was barely detectable in gastric cancer cell lines (Figure 3. 1A & 1B). Yun et al. reported that EREG gene expression was low in 7 of 11 gastric cancer cells examined and that this down-regulation was mediated by aberrant CpG methylation of the EREG promoter (Yun et al., 2012).

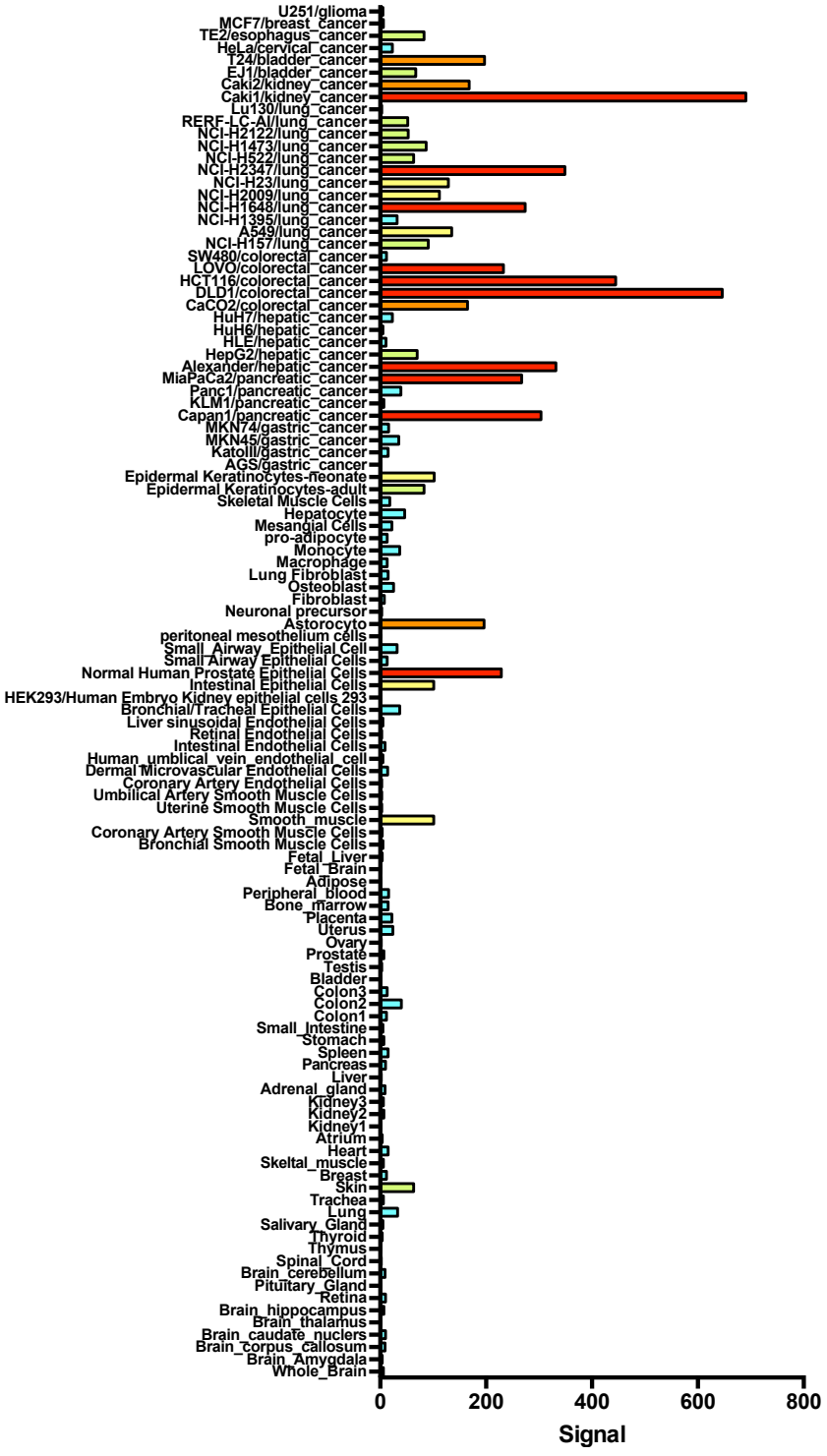

Figure 3. 1A. Expression of EREG genes in RefExA database The relative mRNA expression level of EREG are measured with oligo-nucleotide DNA microarray "GeneChip HG-U133A" in 112 different human normal tissues, normal cultured cells, and cancer cell lines. The detailed information about the tissue sources can be obtained from RefExA database (http://157.82.78.238/refexa/main_search.jsp). Each colored bar represents the gene expression (upper: 200, lower: 0) with red denoting high expression level and blue denoting low expression level.

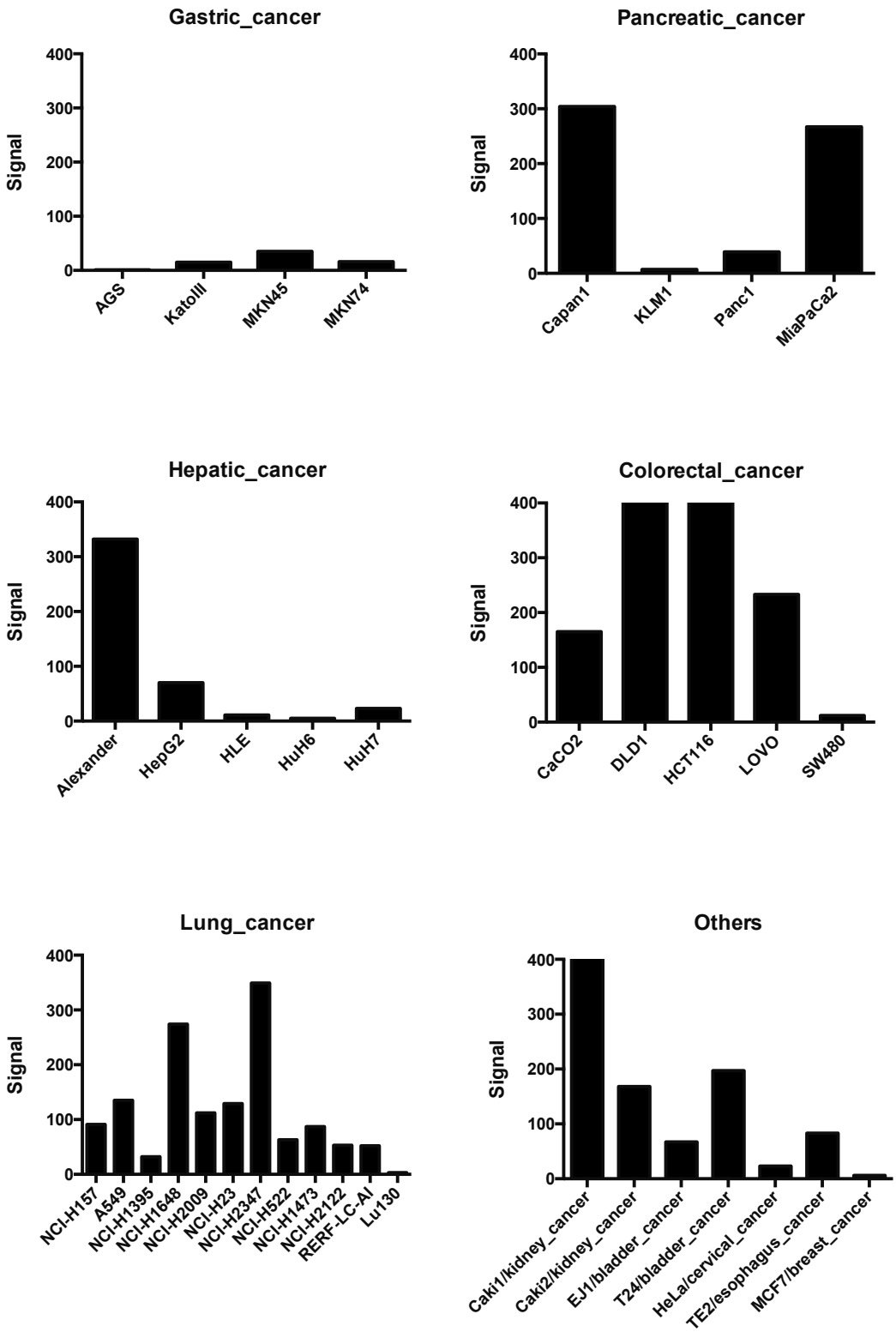

Figure 3. 1B. Expression of EREG genes in RefExA database The figure shows that gene expression RefExA database analysis of relative EREG mRNA levels in various cancer cell lines. DNA microarray mRNA levels of EREG are plotted on the y-axis.

3. 2 Generation of anti-EREG antibodies

3. 2. 1 3D structure modeling of 9E5 antibody

For the variable region of 9E5, the top twenty sequences were identified according to the FR identity index (defined as having >70% sequence identity). Global alignment was manually carried out by adjusting for differences in the CDRs and a first ranking was performed based on sequence identity (ignoring the CDRs). For 9E5 VH and VL, 10 and 4 sequences, respectively, were found to have >90% FR identity. The crystallographic resolution and the source of top 10 selected variable domain sequences for 9E5 VH and VL, respectively, were assessed (Table 3. 1). Table 3. 1 summarizes the most sequence homologous template (identified by BLAST) for each antibody segment [VH and VL frameworks (FRH and FRL), CDRs L1, L2, L3, H1, H2 and H3]. In a series of selectable panes, the table also shows the top ten templates for each antibody segment.

Table 3. 1. Ranking of the PDB antibody variable domain sequences with more than 70% framework sequence identity with 9E5

(A) Ranking for light chain

		Without CDRs (length = 58)			
Ranking, VL	PDB-code	Identity (%)	Mismatches	Resolution (Å)	Source
1	2ADF	98	1	2	Mouse
2	3I75	93	4	2	Mouse
3	2E27	93	4	2	Mouse
4	1EAP	93	4	3	Mouse
5	1FJ1	90	6	3	Mouse
6	1R0A	84	9	3	Mouse
7	1FNS	84	9	2	Mouse
8	1OAK	84	9	2	Mouse
9	1JV5	83	10	2	Human
10	3CX5	79	12	2	Mouse

(B) Ranking for heavy chain

		Without CDRs (length = 63)			
Ranking, VH	PDB-code	Identity (%)	Mismatches	Resolution (Å)	Source
1	3T3P	95	3	2	Mouse
2	3NIG	95	3	2	Mouse
3	3NID	95	3	2	Mouse
4	3NIF	95	3	2	Mouse
5	2VDR	95	3	2	Mouse
6	2VDO	95	3	3	Mouse
7	3T3M	95	3	3	Mouse
8	2VDQ	95	3	3	Mouse
9	2VDP	95	3	3	Mouse
10	2VDL	95	3	3	Mouse

(C) Summary of homology modeling

SUBJECT-ID	PDB-code	Identity (%)	alignment-length	Mismatches	Resolution (Å)	Source
FRL	2ADF	98.28	58.00	1.00	1.90	Mouse
FRH	3T3P	95.24	63.00	3.00	2.20	Mouse
LIGHT	2ADF	98.96	96.00	1.00	1.90	Mouse
HEAVY	2RCS	87.85	107.00	9.00	2.10	Mouse
L1	2ADF	100.00	11.00	0.00	1.90	Mouse
L2	2ADF	85.71	7.00	1.00	1.90	Mouse
L3	2ADF	100.00	8.00	0.00	1.90	Mouse
H1	1J05	100.00	10.00	0.00	1.50	Mouse
H2	3Q3G	94.12	17.00	1.00	2.70	Mouse
LIGHT_HEAVY	1EAP	76.92	208.00	46.00	2.50	Mouse

The antibody 3T3P (PDB codes) showed 95% FR identity with 9E5 VH and the antibody 2ADF (PDB codes) showed 98% FR identity with the 9E5 VL. Further, the CDRs of the light

chain (L1, L2, and L3) of 2ADF (86–100% sequence identity) were very similar to 9E5, and CDRs 1 and 2 of the heavy chain of 9E5 templates, i.e., 1J05 (100% sequence identity) and 3Q3G (94% sequence identity), were chosen for H1 and H2, respectively. All CDRs, except H3, were modeled using templates from PDB, whereas CDR-H3 was remodeled de novo by using a kinematic loop modeling algorithm in a Rosetta protocol (Sivasubramanian et al., 2009). After homology modeling, the best discrete optimized protein energy score result was further optimized to establish the final 3D model of 9E5 by using energy minimization (Figure 3. 2).

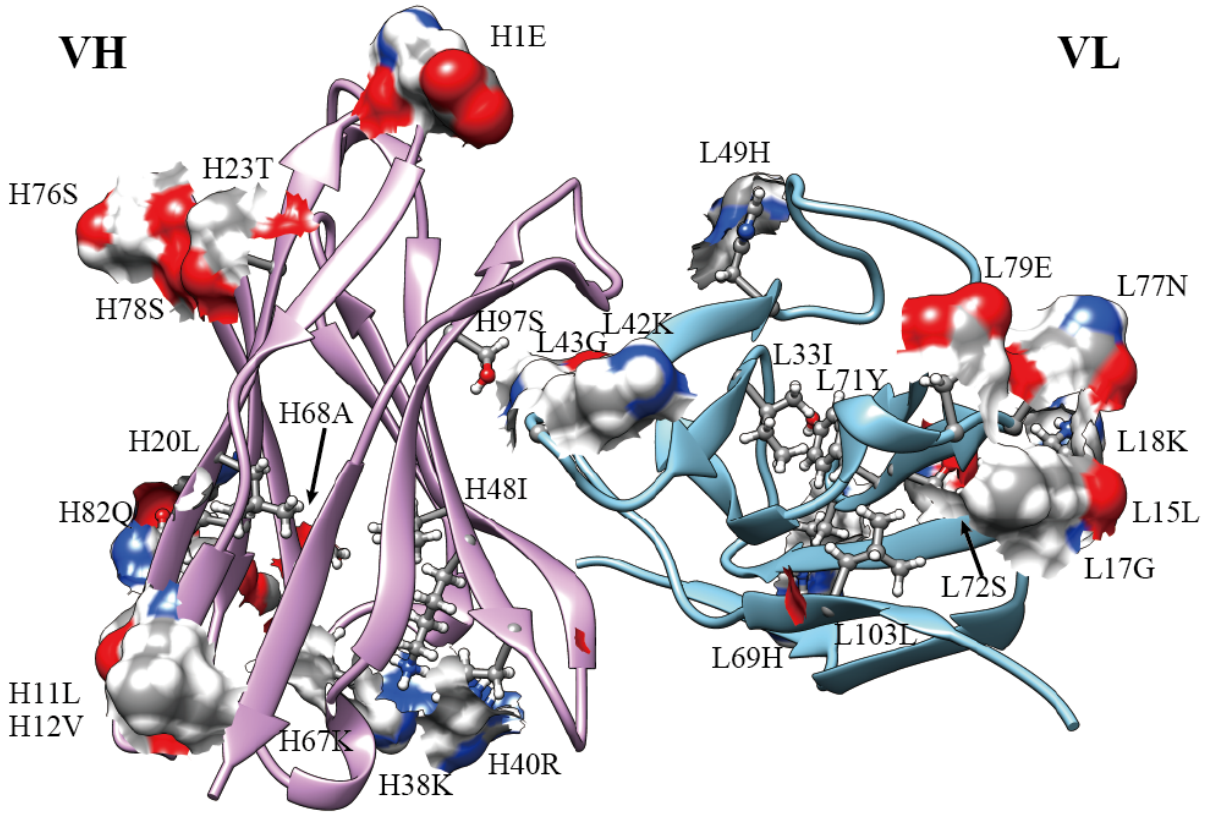

Figure 3. 2. View of the 9E5 variable region constructed by homology modeling The surface framework residues that are non-human-like and that are therefore preferably mutated to 'human' amino acids are in Jmol element colors. In the VH (pink) fourteen amino acids should be humanized whereas in the VL (light blue) thirteen amino acids should be humanized.

Additionally, the crystal structure of 9E5 in apo-form and complexed with its antigen were resolved (Kado et al., manuscript in preparation); the similarities between the crystal structure and the model will be discussed in a separate report. However, the structure of the CDR-H3 loop was taken not to fit that may contribute to the structural features of binding function as a surface antigen and 9E5.

3. 2. 2 Humanization of 9E5 antibody

Using the modeled 9E5, this study identified residues to be mutated to obtain HM0. Additionally, a human target sequence homologous to 9E5 variable regions was identified by searching the immunoglobulin Genbank database. Surface positions of 9E5 displaying nonhuman residues were identified by combining the information on the surface-exposed positions with an alignment of the most homologous human variable region sequence (Figure 3. 3).

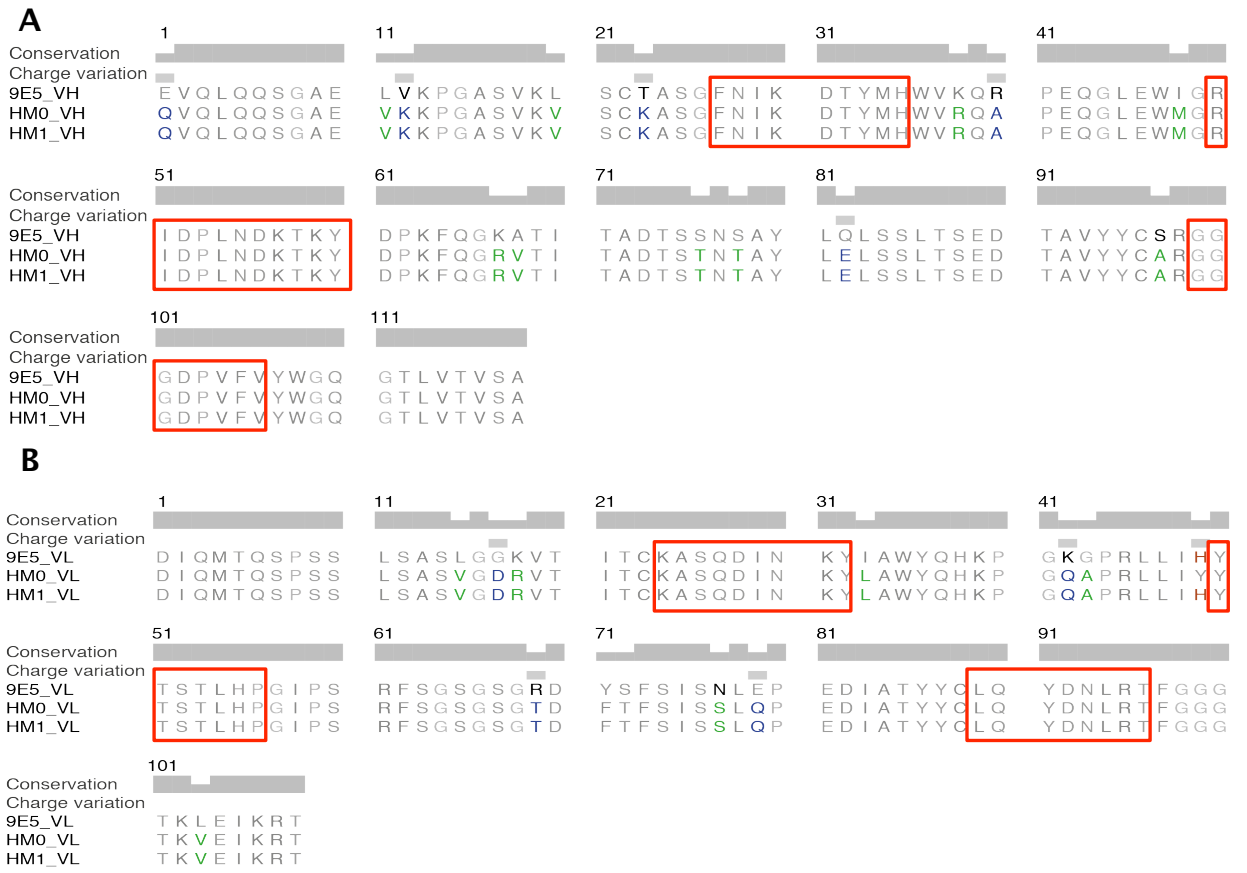

Figure 3. 3. Amino acid sequences of anti-EREG antibodies heavy (A) and light (B) chain variable regions 9E5_VH and 9E5_VL indicate heavy and light chain variable regions of murine 9E5 monoclonal antibody, respectively. HM0_VH and HM1_VH indicate different versions of humanized heavy chain variable regions. HM0_VL and HM1_VL indicate different versions of humanized light chain variable regions. The CDRs are enclosed with red brackets. CDR sequences that were fixed as the template sequence (WT) are shaded in gray. The identical residues between the mouse and human consensus sequences are marked by gray and differed residues are marked by blue (charge variation) or green (non-charge variation).The residues that were reconstituted during humanization are indicated in red.

Fourteen of the nonhuman residues in HM0-VH were surface residues, and 13 of the nonhuman residues in HM0-VL were also surface exposed. Within these candidates, five residues (H1Q, H12K, H23K, H40A, and H82E) in VH and five residues (L17D, L42Q, L49Y, L69T, and L79Q) in VL were mutated. These changes would affect the charge of the antibody

(amino acids are identified by their chain, H or L, the single-letter amino acid code, and their position in the sequence).

Other candidates with differential residues were considered; for these, the structures of side chains would become smaller, but the physical and chemical characteristics related to charge, hydrophobicity, and polarity would be similar (Appendix A2). However, this result indicated that the initial version of the humanized antibody (HM0) lost its binding activity (Table 3. 4), likely due to mutations near the antigen-binding site. Thus, I sought to identify mutated residues that played an important part in constructing the CDR loops following mutation to their respective human consensus sequence. Of these, six FR residues (H23K, H38R, H48M, H97A, L33L, and L49Y), which were near the CDRs (within ~5 Å), were identified. Additional modeling revealed that L49Y produced some rearrangements of the neighboring side chains and possibly modified the overall conformation of the CDR-L2 loop (Figure 4. 2A). Other FR residues produced either stabilized the conformation of CDR loops or did not bind to EREG. Therefore, L49Y was "back-mutated" into the first humanized construct to obtain the HM1 antibody.

3. 2. 3 Genetic construction of the 9E5 variable region

The 9E5 gene segments were first cloned by PCR and sequenced. The variable region genes were then simultaneously humanized by gene conversion mutagenesis using preassembled oligonucleotides. The genetic segments of HM0-VH/VL were sub-cloned into the restricted cleavage pCET1019-HS-puro to form pHM0VH-1/pHM0VL-1. Additional humanized variant (HM1) was constructed by site-directed mutagenesis of pHM0VH-1/pHM0VL-1. Each vector

contained human IL2 signal sequence (Sasada et al., 1987) and coding sequence of the human IgG1, including the constant hinge, CH2, and CH3 regions. The intracellular cleavage of the IL2 signal peptide leads to the secretion of the immunoglobulin chain.

3. 2. 4 Humanized antibody expression, purification, and quantification

The humanized anti-EREG antibodies were purified from CD FortiCHO™ medium, as described in Section 2. 5. 4. The purified antibody was buffer-exchanged against PBS and concentrated to 50–100 μL. The purity of the sample was confirmed by the detection of a single band in SDS-PAGE gels performed under non-reducing conditions (Figure 3. 4).

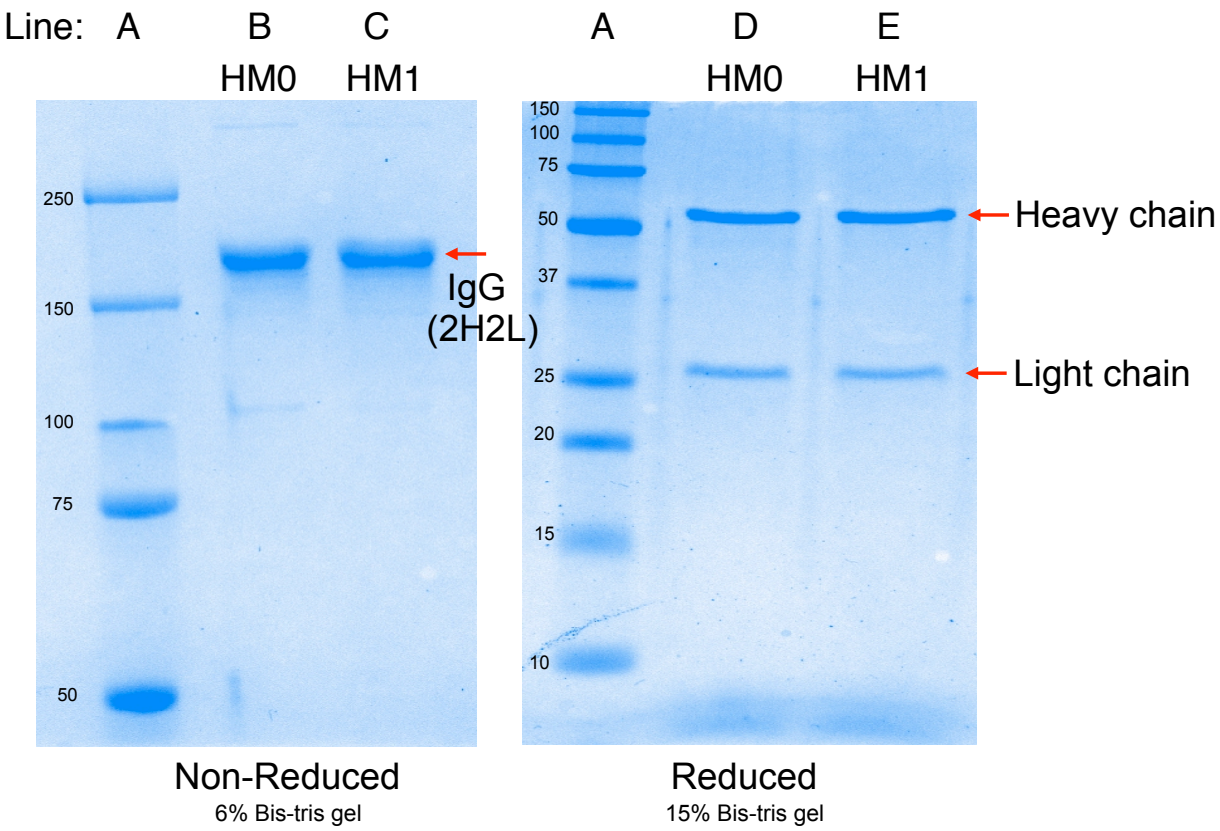

Figure 3. 4. SDS-PAGE analysis of the purified humanized anti-EREG antibodies.
Line A: Molecular weight marker
(from top to bottom: 250 kDa, 150 kDa, 100 kDa, 75 kDa 50 kDa, 37 kDa, 25 kDa, 20 kDa, 15 kDa and 10 kDa,)
Line B & C: Completely assembled humanized anti-EREG molecule in 6% Bis-tris gel under non-reducing condition (without treatment with beta-mercaptoethanol)
Line D & E: Heavy chain and light chain of 1 μg humanized anti-EREG (Line C) in 15% Bis-tris gel under reducing condition (Inter-chain disulfide bonds were reduced by heating for 5 min at 90 °C in loading buffer containing 1% beta-mercaptoethanol)

In the presence of beta-mercaptoethanol added to reduce the humanized anti-EREG antibody, the heavy and light chains detected by SDS-PAGE were of expected molecular weight (~55 kDa for the heavy chain and ~25 kDa for the light chain). The migration patterns of heavy chain and the light chain of the humanized anti-EREG antibodies were similar to that of a human IgG antibody (Figure 3. 4). Two polypeptides of approximately 55 and 25 kDa, corresponding to

the heavy and light chains, respectively, were identified. The clones synthesizing these proteins secreted intact human IgG1 with yields from 4 to 10 μg/mL per 10^6 cells (data not shown). The expression level of humanized anti-EREG antibodies was approximately 100 μg of secreted humanized anti-EREG antibodies per liter of the supernatant after 24 days of culture in CD FortiCHO™ medium with feeding medium.

3. 3 Immunogenicity of humanized antibodies

Monoclonal antibodies approved by the FDA were engineered to be humanized or prepared as human, are shown in Table 3. 2 (Koren et al., 2002).

Table 3. 2. Incidence rate of antibodies to therapeutic antibodies

Antibody	Antibody type	incidence
Oncoscint® (anti-TAG)	murine IgG1	55%
OKT®3 (anti-CD3)	murine IgG2a	80%
Rituxan® (anti-CD20)	chimeric IgG1	< 1%
Simulect® (anti-IL2Ra)	chimeric IgG1	< 2%
ReoPro® (anti-GPIIb/IIIa)	chimeric IgG1 Fab	7-19%
Remicade® (anti-TNF)	chimeric IgG1	10-57%
Erbitux® (anti-EGFR)	chimeric IgG1	5%
Synagis® (anti-RSV)	humanized IgG1	< 1%
Herceptin® (anti-HER2)	humanized IgG1	0.1%
Zenapax® (anti-IL2Ra)	humanized IgG1	8%
Campath® (anti-CD52)	humanized IgG1	< 2%
Avastin® (anti-VEGF)	humanized IgG1	None detected
Humira® (anti-TNF)	human IgG1 (phage)	> 5%

- Antigenicity is not dependent on the rate of humanization
- Reducing antigenicity is necessary through optimization process of the candidates

*Adapted from Current Pharmaceutical Biotechnology 3, 349-360 (2002) (Koren et al., 2002).

Humanization of monoclonal antibodies were performed to prevent or reduce the incidence of HAMA (human anti-mouse antibody) or HACA (human anti-chimeric antibody) effects, ranging from mild allergic reactions to anaphylactic shock, that frequently occur with mouse and chimeric therapeutic monoclonal antibodies. Chimeric antibodies were engineered by fusing murine variable regions with human constant regions taken from the kappa light chain and the

IgG1 heavy chain. The chimeric antibodies, approximately 65% human, showed reduced immunogenicity. Humanized anti-EREG antibodies (HM0 & HM1), about 95% human, were produced by grafting only the murine CDR hypervariable loops into human antibody frameworks (Table 3. 3).

Table 3. 3. Comparison of the immunological forms of monoclonal antibodies

	9E5 antibody (Murine)	Chimeric antibody	HM0 & HM1 antibody (Humanized antibody)
Murine amino acid	1326/1326	452/1326	104/1326
	100%	35%	**<5%**
Incidence of HAMA	55-80%	5-10%	**0-2%**

Interestingly, within the subclass of currently approved fully human antibodies, the proportion of those with negligible, tolerable, and marked immune responses is not substantially different from those of humanized antibodies (Table 3. 2). In a subset of patients, Adalimumab (Humira®) has been reported to induce neutralizing responses that varied depending on the disease and therapy (5–89%) (Bender et al., 2007). Given the ability of the human immune system to mount anti-idiotype antibodies, this is not surprising. Therefore, fully human antibodies may have reached the limit of ability to select for reduced immunogenicity antibodies without more directed engineering.

3. 4 Analysis of anti-EREG antibodies

3. 4. 1 Binding of anti-EREG antibodies to EREG

The applicability of each antibodies in immunoblotting was examined. To increase the sensitivity of detection, prior to western blot analysis, cell lysates prepared from DLD-1, HCT116 (cell line with high expression of EREG), and AGS (cell line with low expression of EREG) were subjected to immunoprecipitation with various antibodies. As shown in Figure 3. 5, the antibodies 9E5, HM0, and HM1 helped detect EREG in cell lysates, while the control antibody failed to immunoprecipitate EREG. These antibodies specifically recognized a non-glycosylated propeptide form (Baba et al., 2000) with an apparent molecular weight of ~19 kDa expressed in the DLD-1 and HCT116 cells (Figure 3. 5), but not in the AGS cells (Figure 3. 5). Additionally, the result indicated a significantly lower ability of HM0 to bind to EREG. The binding specificity was further examined by analyzing the cell surface expression and subcellular localization of EREG using each antibody.

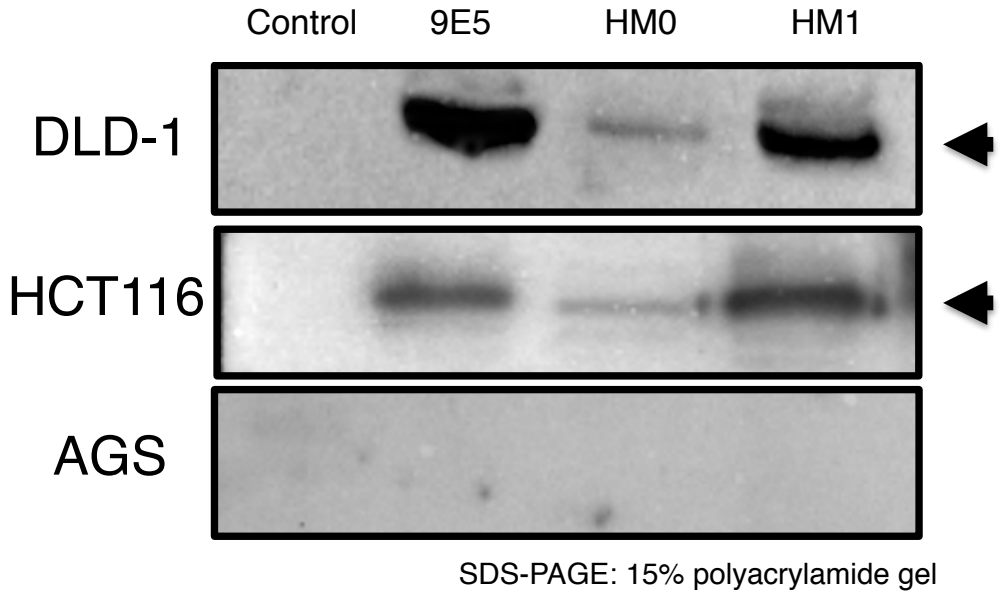

Figure 3. 5. Immunoprecipitation Immunoblot detection of EREG in the cell lysates were immunoprecipitated with each antibodies (2 μg/mL in 9E5, HM0, and HM1, respectively). The samples were subjected to western blot analysis. Control, 1 mL of the cell lysates were immunoprecipitated with normal mouse IgG; 9E5, 1 mL of the cell lysates were immunoprecipitated with 9E5 IgG; HM0, 1 mL of the cell lysates were immunoprecipitated with HM0 IgG; HM1, 1 mL of the cell lysates were immunoprecipitated with HM1 IgG. The arrowhead indicates the mobility of mature epiregulin on SDS-PAGE.

3. 4. 2 Binding of antibodies to EREG expressed on the cell surface and subcellular localization

In an attempt to better understand the binding activity of antibodies, the cell surface and subcellular localization of EREG was examined by immunofluorescence staining. For this purpose, antibody-binding assays were performed using colorectal carcinoma cells (DLD-1, HCT116) and gastric cancer cells (AGS). Bound 9E5 and HM1 were detected predominantly as intense green florescence spots on the cell surface with some faint fluorescence, showing the

subcellular distribution of EREG in colon cancer cells (Figure 3. 6A and 5C). HM0 showed a diffuse cell surface staining (Figure 3. 6B).

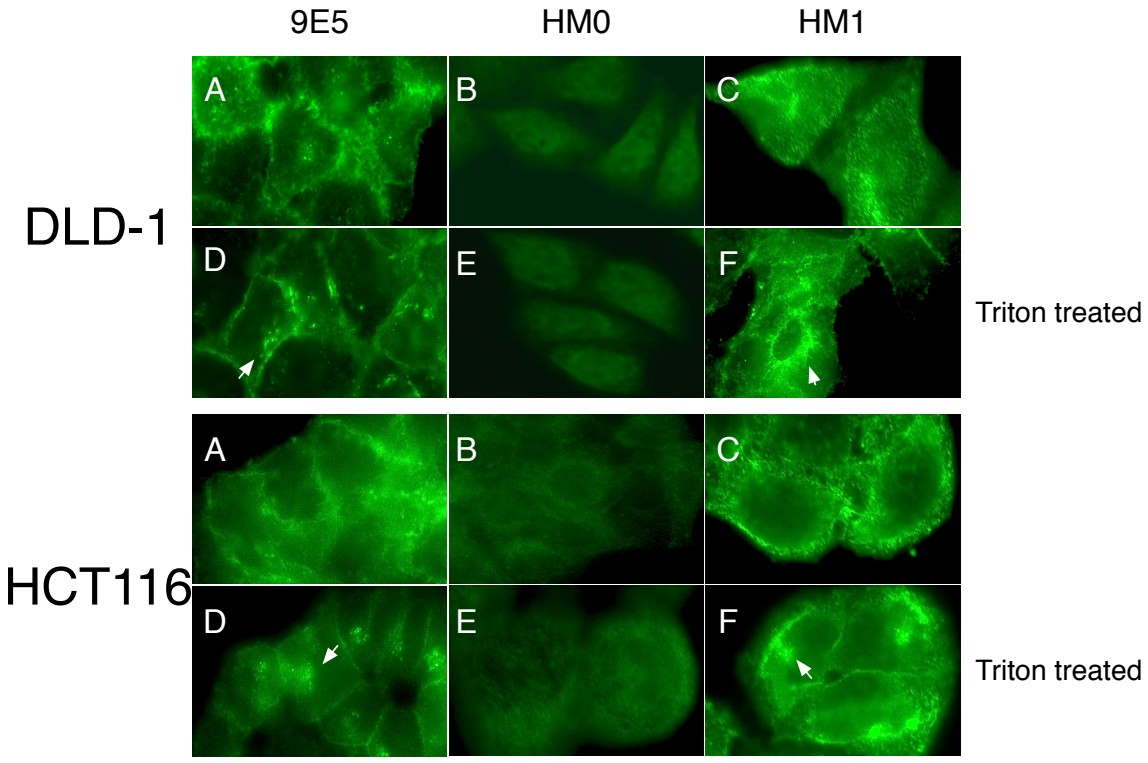

Figure 3. 6. Immunofluorescent staining of antibodies in human colorectal carcinoma cells Human colorectal carcinoma cells, DLD-1 and HCT116, were fixed with paraformaldehyde and treated with 0.2% Triton X-100 solution (localization to endomembranes was observed; white arrow) or not treated at all. Immunization was performed using each antibody, followed by visualization with an Alexa Fluor 488 labeled secondary secondary anti-mouse antibody as described in Materials and Methods.

These results confirmed the antibody-binding activity as well as the on the cell surface distribution of EREG in colon cancer cells. To examine if the antibodies were endocytosed along with the EREG, cells were labeled with antibodies recognizing the intracellular domain of the EGFR (unpublished data). Binding assay was also performed in gastric cancer cells. The results

indicated that none of the antibodies showed binding to AGS cells (data not shown). I further analyzed the subcellular localization of EREG under permeabilization conditions. In both colon cancer cell lines labeled with 9E5 and HM1, specific staining was observed in the endoplasmic reticulum (ER) and Golgi bodies (Figure 3. 6D, 6E, and 6F). To confirm this, 9E5 and HM1 were recognizing a synthetic EREG peptide corresponding to a portion of the sequence of the mature form domain of the premature EREG (unpublished data) (Figure 3. 7).

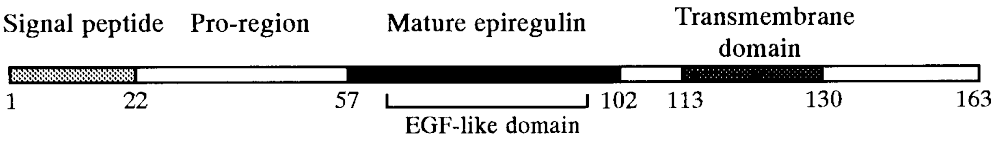

Figure 3. 7. Schematic diagram of the structural organization of EREG precursor (Toyoda et al., 1997)

3. 4. 3 Binding efficiency of anti-EREG antibodies analyzed by flow cytometry

The cell surface-binding efficiency of each antibody to EREG-expressing cells was determined by flow cytometry as described in Section 2. 6. 4. DLD-1 and HCT116 cells were used as EREG-positive cells, and AGS cells were used as a negative control. Binding efficiency was tested by adding various concentrations (0–1 μg/mL) of each antibody to cells, followed by staining with Alexa Fluor 488-labeled antibodies and flow cytometry. Data corresponding to 0.1 μg/mL antibody is shown in green line, blue line indicates data corresponding to 0.5 μg/mL antibody, and purple line shows data corresponding to 1 μg/mL of antibody. Negative controls (0 μg/mL) are shown in red. The results of flow cytometry indicated that the EREG-positive population of DLD-1 and HCT116 cells tested with HM1 were obviously superior to those of

same concentration of HM0 (Figure 3. 8A).

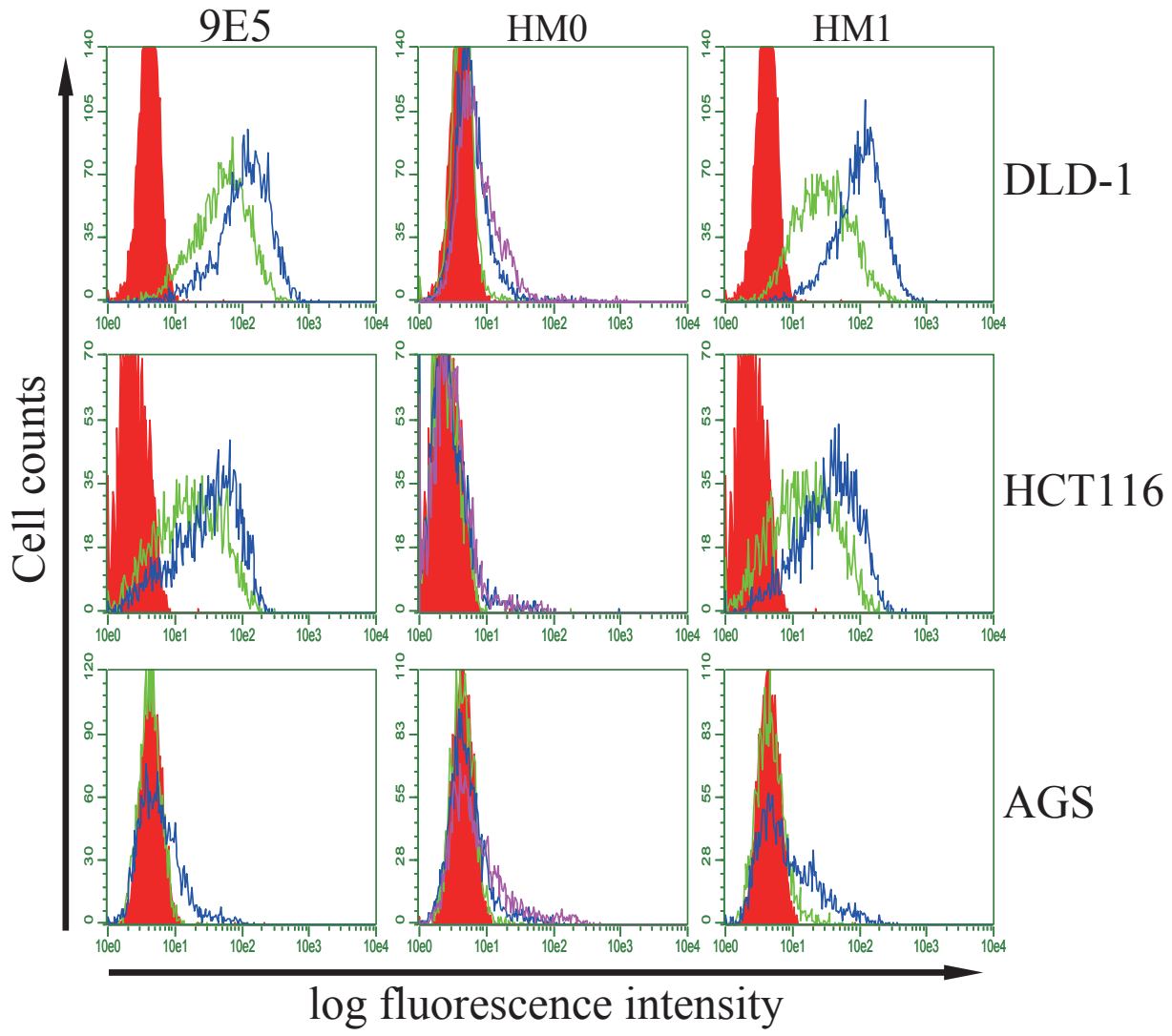

Figure 3. 8A. Flow cytometry analysis Antibodies were tested for their ability to bind cells by using each cell line (DLD-1, HCT116, and AGS). Cell lines were resuspended in FACS buffer and were incubated in the presence or absence of 0.1, 0.5, and 1 μg of antibodies for 1 h at ice in the dark. The binding ability of antibodies was analyzed by FACScan analysis. Green line: 0.1 μg/mL, blue line: 0.5μg/mL, purple line: 1 μg/ mL, red line: negative control (0 μg/mL). Data are representative of three independent experiments, all with similar results.

As shown in Figure. 3. 8, a significant shift in fluorescence intensity was also observed for 9E5. In order to quantitatively compare the performances of each antibody, the mean fluorescent intensities (MFI, obtained by analyzing the histogram statistics) were plotted compared to the control (Figure 3. 8B).

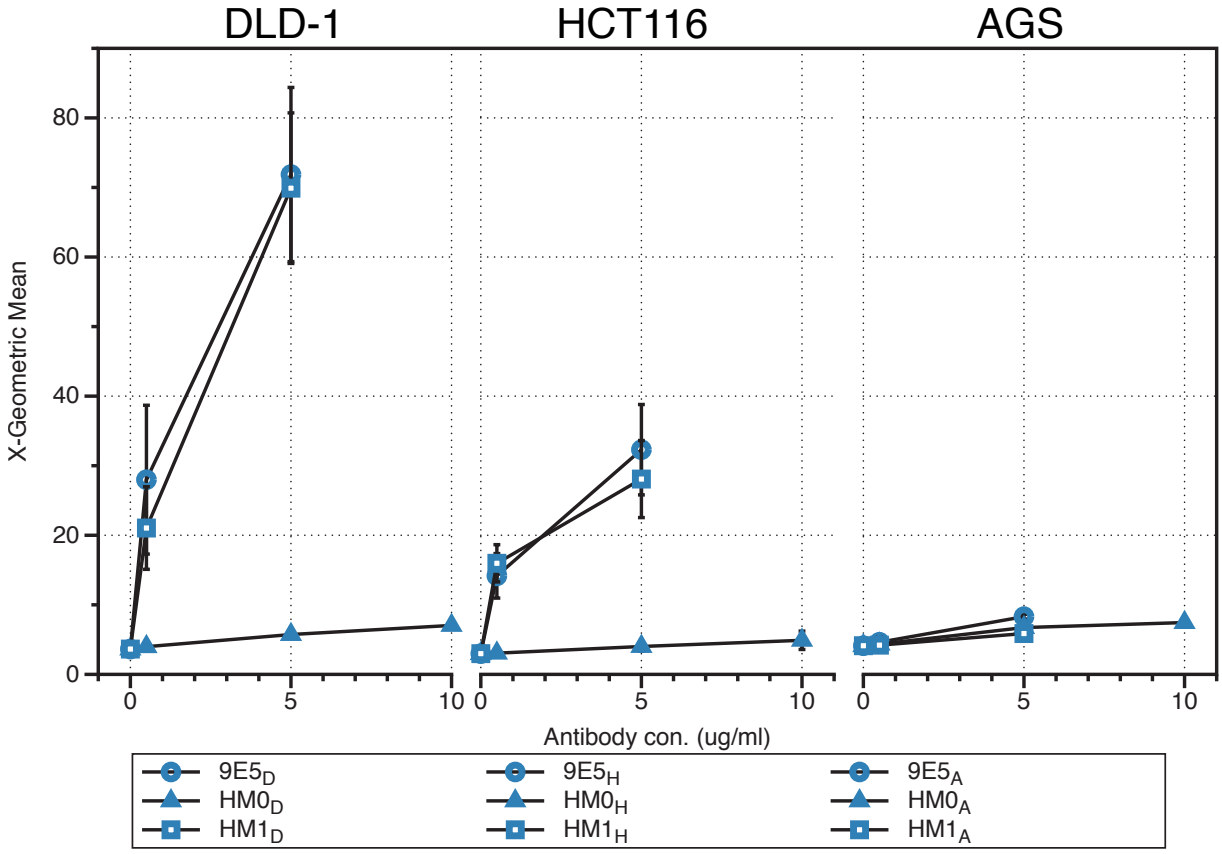

Figure 3. 8B. Geometric mean values for binding ability on each cell surface were measured several times. Statistical analysis of binding ability in each cell lines.

The binding efficiency was found to be dependent on the concentration of the antibody used. Significantly, HM1 antibody was able to bind to EREG-expressing cells at a relatively low

concentration (0.1 μg/mL) at which HM0 showed no binding. Furthermore, at similar concentrations, the binding efficiency of HM1 was higher than that of HM0.

3. 4. 4 Affinity measurements by surface plasmon resonance (BIAcore)

Interactions between EREG and various antibodies were compared by real-time analyses of biomolecular interactions (Surface Plasmon Resonance, BIAcore T200). Binding affinity and kinetics of human epiregulin-Fc (=analytes) to each antibody coupled as ligand to a CM5 sensor chip were measured. Initially, several potential regeneration conditions (acidic, high salt, addition of chelator or detergent) were tested for incomplete removal of human epiregulin-Fc from the biosensor with immobilized antibody. Additionally, in all cases, a reduced antibody activity was observed in each subsequent measurement (data not shown). Therefore, all BIAcore data reported in this study were obtained from single-cycle kinetic experiments. In single-cycle mode, the analyte is injected in increasing concentrations within a single scan and without surface regeneration between injections. Importantly, both modes provide very similar kinetic rate constants (Trutnau, 2006). Figure 3. 9 shows the experimental sensorgrams obtained, association of the analyte with the ligand proceeded for 120 sec, and dissociation in analyte free buffer was typically 600 sec. The kinetic rate constants (k_{a1}, k_{a2}, k_{d1}, and k_{d2}), as well as equilibrium dissociation constant (K_D), were estimated by global fitting analysis of the titration curves to the bivalent analyte model. The results of this analysis are summarized in Table 3. 4. The table parameters were determined by Biacore analysis and are expressed as mean ± SD values.

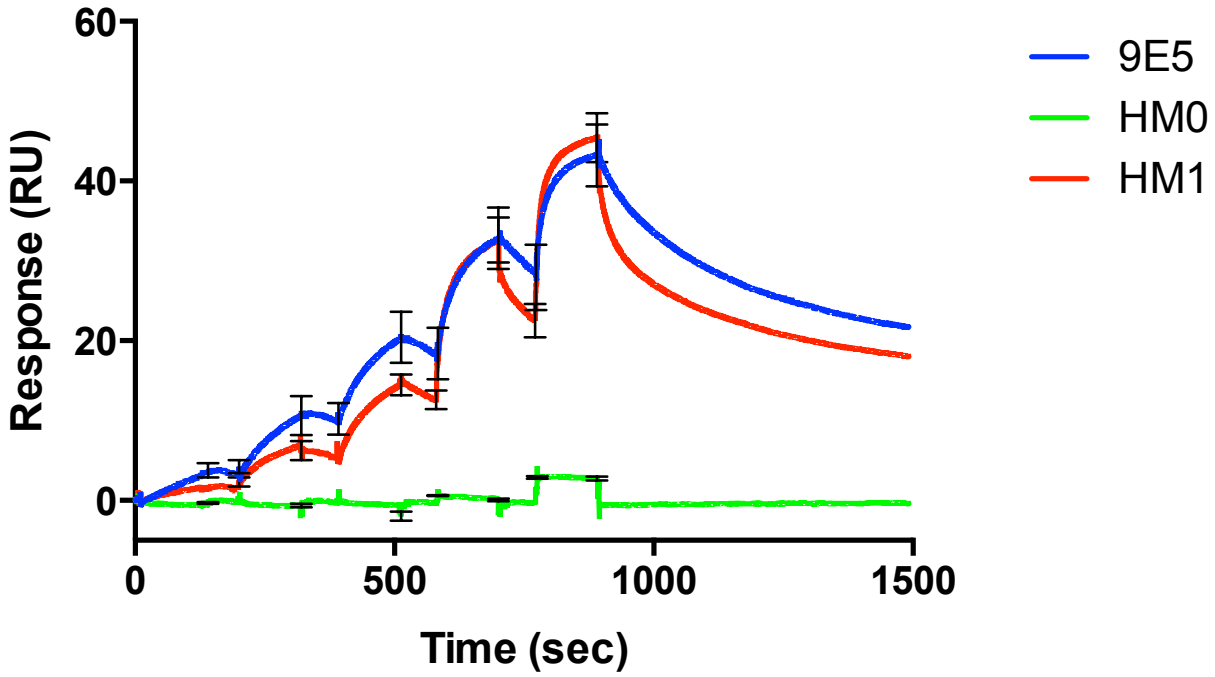

Figure 3. 9. Single-cycle kinetic analysis of 9E5, HM0, and HM1 antibodies binding amine-coupled CM5 chip on Biacore. hEpiregulin-Fc was injected as a five-membered fivefold series with highest concentrations of 1.5 µM, 300 nM, 60 nM, 12 nM, and 2.4 nM, respectively, and analyzed in duplicate binding cycles over three differing capacity reaction surfaces.

Table 3. 4. Kinetic parameters for anti-EREG antibodies

Antibody	k_{a1} (1/Ms)	k_{a2} (1/Rus)	k_{d1} (1/s)	k_{d2}(1/s)	K_D(M)
9E5	$3.42 \pm 1 \times 10^{5}$	$2.45 \pm 0.2 \times 10^{-3}$	$4.07 \pm 2 \times 10^{-3}$	$3.62 \pm 0.6 \times 10^{-2}$	$3.68 \pm 0.6 \times 10^{-8}$
HM0	$6.12 \pm 2 \times 10^{4}$	$3.37 \pm 0.9 \times 10^{-6}$	$5.30 \pm 1 \times 10^{-3}$	$7.16 \pm 0.3 \times 10^{-4}$	$8.33 \pm 1 \times 10^{-7}$
HM1	$2.98 \pm 1 \times 10^{5}$	$2.52 \pm 0.2 \times 10^{-3}$	$3.47 \pm 3 \times 10^{-3}$	$3.19 \pm 0.8 \times 10^{-2}$	$4.53 \pm 0.9 \times 10^{-8}$

Good fitting of experimental data to the calculated curves was observed, suggesting that the fitting model was correct. Generally, HM1 showed slower off-rates than HM0. HM1 showed a lower apparent K_D that was 20-fold lower than that of HM0. Additionally, HM1 and 9E5 showed binding kinetics similar to that of human epiregulin-Fc, with the binding affinities measured being 45 nM and 37 nM, respectively.

The above data indicated that the importance of VL residue 49 is supported the observed to preserve their affinity for EREG on replacement of histidine in HM1 with the corresponding humanized residue, tyrosine (HM0). The results of these binding studies allowed us to prove that the FR-CDR interactions in the resurfaced L49H and HM1 antibody preserved the native conformations of the CDRs. Therefore, FR residues must be considered when designing a humanized antibody.

3. 4. 5 ADCC assay

ADCC is important for the *in vivo* activity of many therapeutic monoclonal antibodies. Thus, this study assessed the ADCC activity by using Jurkat NFAT luciferase reporter cells, as described in Section 2. 6. 6. The cellular cytotoxicity of each antibody to colon cancer cells (DLD-1 and HCT116 cells) with enhanced FcγRIIIa binding was evaluated (Figure 3. 10).

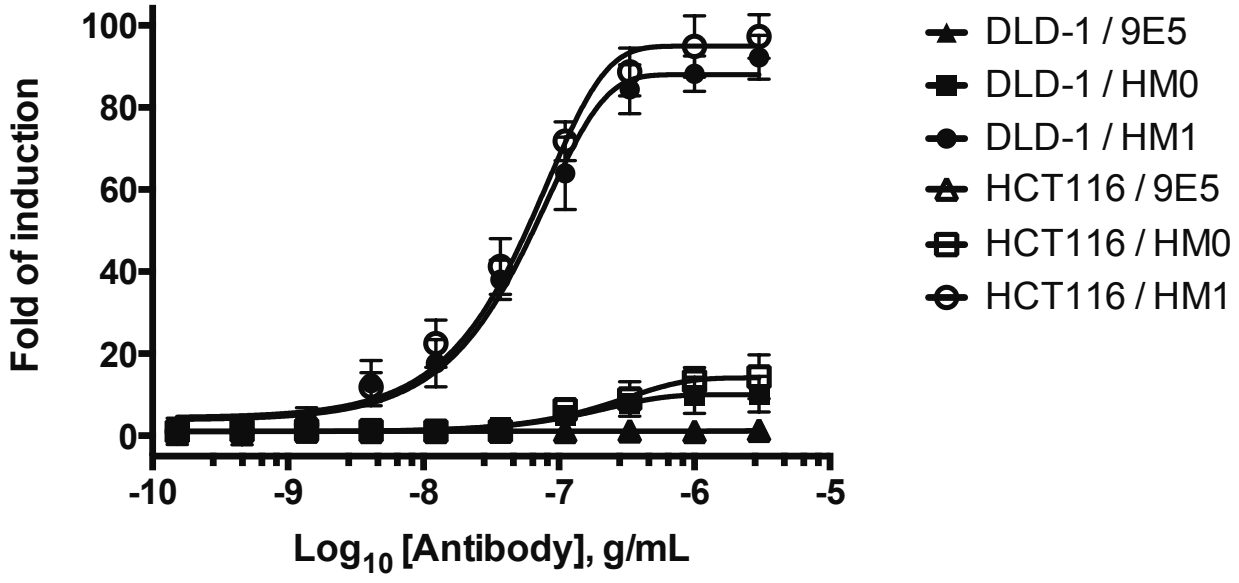

Figure 3. 10. Anti-EREG antibodies were induced NFAt driven luciferase activity in Jurkat cells expressing human FcγRIIIa. The figure is a composite of three independent assays, error bars ± standard deviation. Data were fitted using the 4PLC curve fit of the GraphPad Prism software.

Subsequently, I generated humanized anti-EREG antibody (HM1) and examined their effector properties. Analysis of the ADCC using DLD-1 cells revealed that HM1 exhibited the highest levels of cellular cytotoxicity, a 90-fold increase in cytotoxicity (induced-background / no antibody control-background) at a concentration of 2 μg/mL, whereas HM0 induced only a 10-fold increase in cytotoxicity at this concentration. However, no significant differences in the ADCCs of 9E5 in colon cancer cells were found with varying concentrations of the antibody. The results of ADCC assay for the 9E5 antibody were inconsistent with those obtained from binding assays.

Chapter 4 Discussion

The objective of this study was to reduce immunogenicity, while maintaining an acceptable level of binding activity of the murine anti-EREG monoclonal antibody through antibody humanization. Therefore, I sought to prepare humanized anti-EREG antibodies with enhanced effector functions and different biological activities, both of which potentiate the clinical response. In this chapter, the method used for molecular targeting of EREG in cancer cells (Section 4. 1), humanization (Section 4. 2), characterization of the humanized anti-EREG antibodies (Section 4. 3), and potential clinical application in cancer therapy (Section 4. 4) are discussed.

4. 1 Molecular targeting of EREG in cancer

In 2008, about 12.7 million individuals were diagnosed with cancer and about 7.9 million deaths occurred because of this disease (Jemal et al., 2011). Its expression, often overexpression, in solid tumors such as head and neck carcinomas, colorectal cancer, prostate cancer, and cancers of the lung and breast has pushed the epidermal growth factor receptor (EGF-R) to become a validated target for anti-cancer therapy (Laskin and Sandler, 2004). Owing to the success of monoclonal antibodies in the past few years, the development of antibody-based methods has become a major therapeutic strategy for fighting cancers (Scott et al., 2012). Food and Drug Administration has approved humanized monoclonal antibodies, including Herceptin® (trastuzumab), Avastin® (bevacizumab), and Synagis® (palivizumab) for clinical trials; these are highly successful in combination therapies. Identification of the mechanism regulating the

proliferation and survival of tumor cells aids the development of novel therapeutics to treat human carcinomas.

A bottleneck in cancer therapy is the specific targeting of cancer cells without affecting normal cells. Potentially, tumor and normal cells may be distinguished by addressing the overexpression of certain tumor-specific markers. Researchers have begun to recognize that the EGF family of proteins may not represent a promising target for cancer therapy because many other growth factors can provide redundant growth-promoting signals. Thus, neutralization of a sole factor triggers compensatory mechanisms (Jones et al., 1986). In fact, several agents directed against specific intracellular or extracellular signaling molecules expressed in tumor cells are currently in clinical development. In most cases, the targets of these agents are also expressed in normal cells. However, this study showed that EREG was expressed only at low levels in normal tissues, but its expression was high in 9 of the 11 human carcinoma cell lines examined (Figure 3. 1A & 1B), suggesting a role for EREG in cancer progression. Therefore, EREG is involved in the development of various human cancers and it has been intensely pursued as a therapeutic target.

Kobayashi and colleagues recently reported that anti-EREG antibodies may be efficacious in the early stages of cancer development, when high levels of cancer stem cells are present (Kobayashi et al., 2012). This suggested that anti-EREG antibodies may be effective for cancer therapy and could be expected to exert synergistic anticancer activities when used with traditional chemotherapeutic agents such as irinotecan for the treatment of colorectal cancer. Different growth-promoting pathways might operate in patients who fail to respond to treatment

with a single drug directed against the ErbB receptors. In this report, I studied different combinatorial strategies that can be employed to improve the efficacy of these drugs.

4. 2 Humanized antibody sequence design

4. 2. 1 Development of a reliable 3D model of the 9E5 antibody

For anti-EREG antibody HM0, the initial version of the humanized antibody was constructed by simply grafting CDRs from the 9E5 light or heavy chain to the light or heavy chain of human antibody. Antigen-binding activity assays showed that this version lost EREG-binding activity. Grafting the CDRs of murine antibodies onto appropriate human frameworks, a more commonly used method, has often resulted in reduced affinity or activity for the target antigen (Jones et al., 1986). Because the CDR grafting method is widely used for humanizing murine antibodies, there are only a few general strategies for recovering the binding affinity of humanized antibodies, and these strategies often require several trial-and-error approaches (Gram et al., 1992).

In this study, a reliable 3D model of the variable regions of the 9E5 antibody was built using computer-aided homology modeling as described in Section 3. 2. 1. Further, the crystal structure of 9E5 in apo-form and complexed with its antigen has been resolved (Kado et al., manuscript in preparation). The similarities between the crystal structure and the molecular model will be discussed in a separate report (Figure 4. 1).

Figure 4. 1. Similarities between crystal and modeled structures Position of the 9E5 modeled (light blue) and the crystal structure (gold) shows that although the overall backbone similarity is high. The red circle is indicated that interaction area between CDR-H3 in 9E5 Fab and N-terminal domain of EREG, there are small shifts in antigen binding site.

The X-ray data of the complex between the antibody and its antigen would be needed to understand the structural basis of this lack of binding affinity.

4. 2. 2 Selection of amino acid residue positions for binding affinity improvement

Although Foote and Winter (Foote and Winter, 1992; Winter and Harris, 1993) defined a "Vernier" zone of framework residues that are important for CDR loop conformation, the necessary mutations should nevertheless be determined experimentally for every antibody. The Vernier zone residues are located in the β-sheet FR regions closely underlying the CDRs and have been known to critically affect antigen binding by directly contacting the antigen, affecting

CDR loop conformation, and/or influencing packing interactions between located in the β-sheet Vernier zone residues probably directly contacting the antigen (covered by the contact CDR definition) were preserved at sites where the sequences differed, while the Vernier zone residues located in the FR regions were changed to those present in the acceptor framework sequence.

In this study, a reliable 3D model of the variable regions of the 9E5 antibody was used to analyze which replacements in the VH/VL framework could have affected the CDRs of the humanized antibody. Six substitution residues (H23K, H38R, H48M, H97A, L33L, and L49Y), made at positions underlying the CDRs, which were suggested to be the main responsible for the total loss of affinity. This study is focused on the L49 residue (L49Y) and FR residues of the CDR-L2 loops because the residues of the mutation-induced conformations differed from those of the mature mAb. The mutation could influence the stabilization of the 9E5 variable region and the conformation of the CDRs and the β-sheet, which fix the structure of the CDR loops (Figure 4. 2A). Additional modeling confirmed that residue L49Y produced some rearrangements of the neighboring side chains and possibly modified the overall conformation of the CDR-L2 loop. In contrast, other FR resides that expected conformational rearrangement of the CDR loop region were not observed. Interestedly, L49H was relatively exposed and in direct contact with the antigen; 2ADF and 1FJ1, for example, were 98% and 90% identical with 9E5, respectively (Figure 4. 2B and 2C). This result may not be expected after database searches since the VL residue 49 is usually tyrosine in human and murine germline VL genes (Figure 4. 2D).

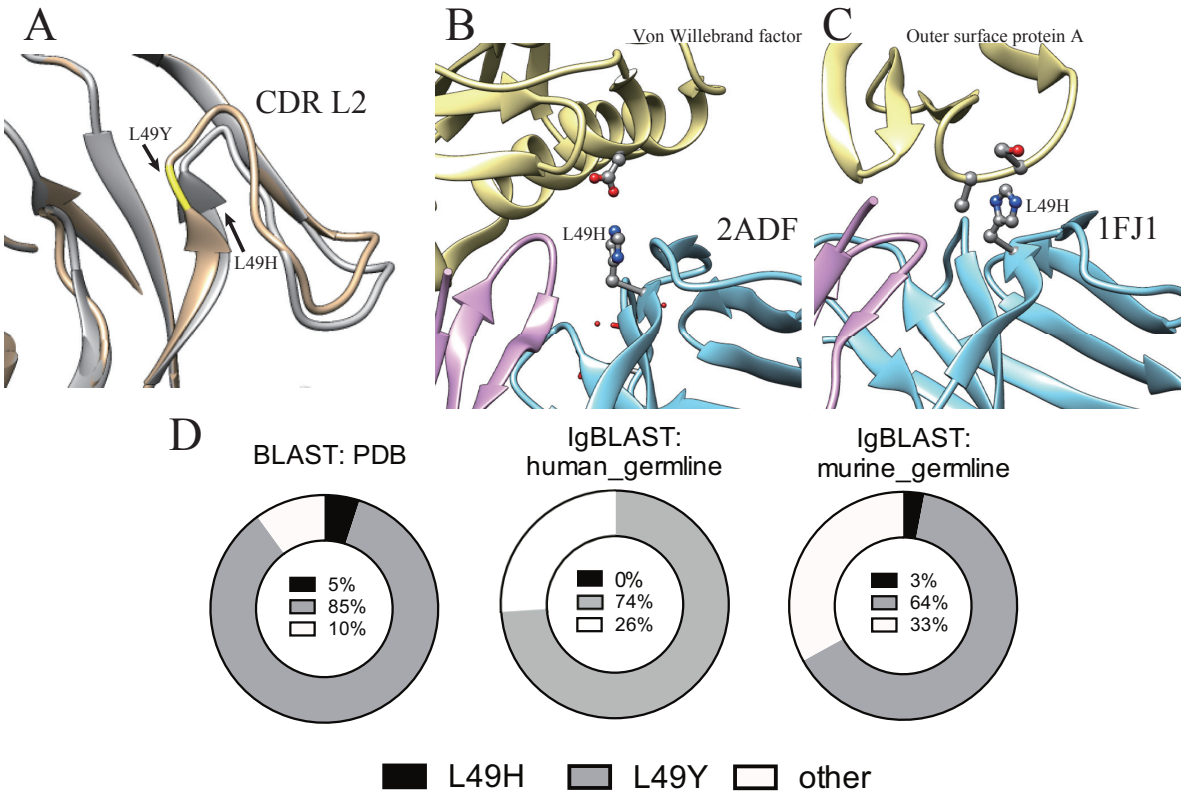

Figure 4. 2. Structural position of L49H residue important for antigen binding (A) Molecular model of the HM0 showing the L49Y residues in relation to the CDR-L2 conformation. The L49H residue is colored dark grey and the mutated L49Y residue is shown in gold.
L49H residue proposed in both structures is shown as grey sticks that may be involved in antigen binding, respectively. (B) 2ADF. (C) 1FJ1. (D) Intrinsic mutation probabilities for VL residue 49 types on the database. BLAST search against the PDB database (left), IgBLAST search against the human germline (center), IgBLAST search against the murine germline (right).

Other investigators have discussed that successful design of CDR grafted antibodies requires that key murine FR residues interacting with the CDRs be substituted into the human acceptor framework to preserve CDR conformations (Padlan, 1994; Makabe et al., 2008).

4. 2. 3 Humanized antibody sequence design

In the humanized anti-EREG antibody, the constant region was cloned from human IgG1 cDNA molecules. For the variable region, the murine CDRs and the important binding-related framework residues were preserved. The other resides were changed to match the selected human consensus framework sequence. As a result, the framework sequence similarity to the human consensus framework sequence was increased from ~63% to ~88%. The humanized heavy chain and light chain frameworks carry 26 and 20 murine residues respectively. When the occurrence frequency of the 46 preserved murine residues were found from the antibody sequence IMGT database (Lefranc, 2004). Furthermore, it is found that 9 of them (H17S, H24A, H43Q, H70I, H72A, H79A, L34A, L73F, and L83I) are conserved in human consensus framework subgroups. For the others, 37 of them 19 (H11L, H12V, H23T, H40R, H48I, H67K, H68A, H82Q, H97S, L15L, L17G, L18K, L33I, L69R, L71Y, L72S, L77N, L79E, and L103L) occur at a frequency rate not less than ~10% in human, and can be considered to have human sequence identities. In addition, all of the preserved murine residues were determined to be potentially buried (H5Q, H17S, H42E, H43Q, H72A, H76S, H87T, L38H, L45R, L74S, and L83I). These buried residues are theoretically less antigenic to B-cell since they are located in a region not directly available to B-cell receptors (membrane bound antibody), although the possible antigenicity of the burred residues to T-cell cannot be excluded.

Examination of the human antibody sequence contained within the database compiled by Abhinandan et al. (Abhinandan and Martin, 2007) showed that a normalized “humanness” score (Z-scores) to be assigned to an antibody sequence. While, by definition, it is the case that every human sequence is 100% human, this analysis shows very clearly that some human sequences

are more typical of the human repertoire (as sampled in the Kabat database) than other sequences. The program search was used to generate pairwise alignments, and the pairwise sequence identities were recorded. These data are plotted in Figure 4. 3, together with equivalent data for mouse–human sequence comparisons.

(A) The Z-score value of the Query sequence is: 0.270

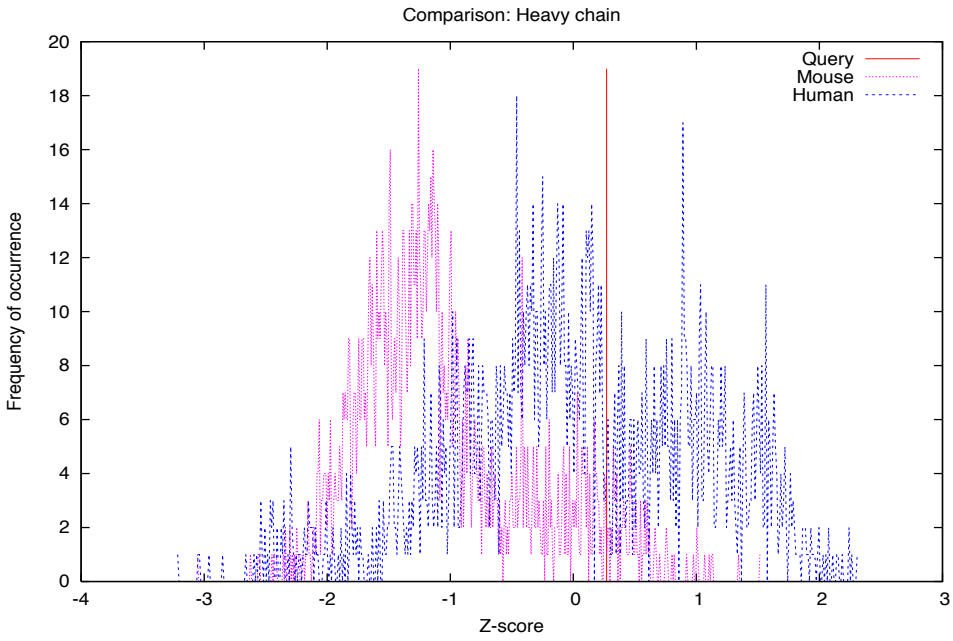

(B) The Z-score value of the Query sequence is: 0.092

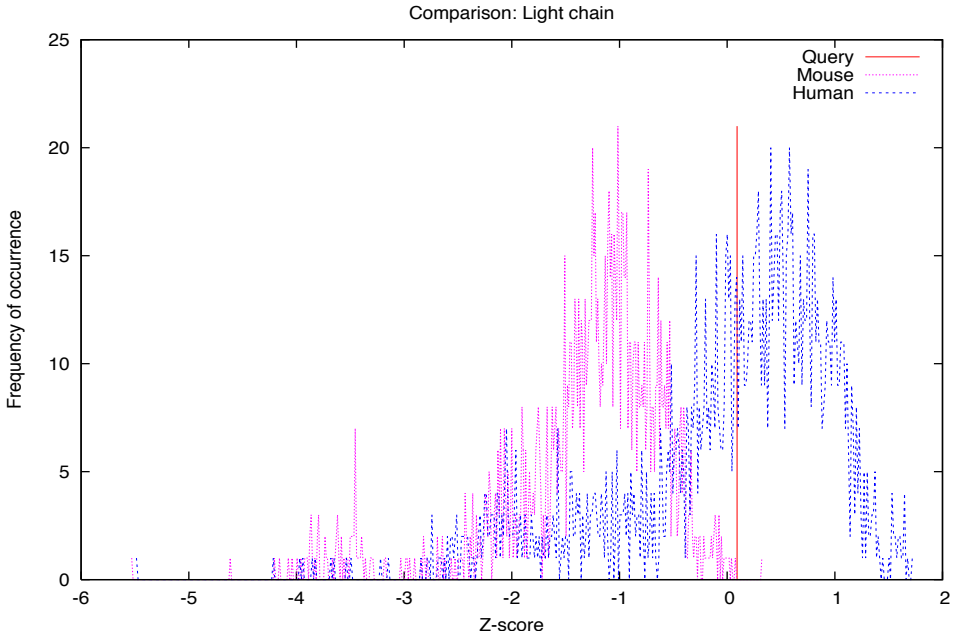

Figure 4. 3. Z-Score analysis: Result of the search against the database of humanized heavy chain and light chain sequences. The humanized antibody sequence are indicated by the vertical lines overlaid on the distribution of humanness scores for all expressed human sequences for (A) HM1 heavy chains, (B) HM1 light chains

The graphs show the results of Z-score analysis. For both humanized heavy and light chains, there is an appreciable shift toward a positive Z-score, indicating an increase in humanness. The humanized antibody (HM1) heavy chain and light chain frameworks showed humanness scores of 0.270 (heavy) and 0.092 (light), respectively (Figure 4. 3). The heavy chain has a similar humanness score to the best humanized antibody shown in Table 4. 1 (HuBrE-3), while the light chain is much higher than the score for Campath-1H. The table shows the data taken from Hwang and Foote (Hwang and Foote, 2005) and adapted from Abhinandan et al.

Table 4. 1. Anti-antibody response (expressed as a percentage of patients who showed a response) and humanness scores for seven humanized and four chimeric antibodies

Antibody	Heavy chain	Light chain	Notes
Humanized			
Zenapax	-0.136	-0.129	Immunosuppressant action
HuBrE-3	0.252	-1.811	Patients may be immunosuppressed
Synagis	-1.708	-0.497	Neonatal
Herceptin	0.965	0.462	Patients may be immunosuppressed
Hu-A33	0.850	-0.401	Patients may be immunosuppressed
Xolair	-0.657	0.309	Immunosuppressant action
Campath-1H	-0.564	-0.009	Patients may be immunosuppressed
Chimeric			
Infliximab	-0.684	-2.237	Immunosuppressant action
Rituximab	-1.350	-1.813	Patients may be immunosuppressed
ch14.18	-1.605	-1.829	Patients may be immunosuppressed
Fully human			
Humira	0.886	0.874	Immunosuppresant action

Both of these antibodies are very well tolerated. Thus, from a perspective of framework sequence analysis, the HM1 humanized antibody can be considered as a human antibody.

4. 3 Characterization of humanized anti-EREG antibodies

In creating a mammalian cell expression system for humanized anti-EREG antibodies, separate heavy chain and light chain expression vectors were constructed. Both vectors contained a human IL2 signal peptide to direct the antibody molecule into the secretary pathway, thus

making it possible for the humanized antibody to be purified directly from the culture supernatant.

Based on the results of concentration measurement (based on a human IgG standard calibration) (Section 3. 2. 4), the antibody expression level in this study was found to be about 5 mg per liter. This expression level is normal when compared with the antibody expression level generally found in a stably transfected CHO cell line. Before evaluating, the humanized anti-EREG antibodies were purified from a protein A column. When the purified antibody sample was subjected to SDS-PAGE analysis under reducing conditions, I found that the purified antibodies sample appeared as a single band (Figure 3. 4). Therefore, the humanized anti-EREG sample was available for experimental use.

In the next step, the binding assays (Section 3. 4. 1) indicated that the humanized anti-EREG antibodies scanned target human colorectal carcinoma cells without cross reactivity to gastric cancer cells, and the results of direct immunofluorescence assay (Section 3. 4. 2) showed that both humanized antibody (HM1) and original murine antibody (9E5) had an antigen-binding pattern similar to that of human colorectal carcinoma cells. The relative binding affinity and efficiency of the humanized HM1 was determined using surface plasmon resonance assay (Section 3. 4. 4) and flow cytometry (Section 3. 4. 3). The results show that HM1 has potency comparable to that of the murine antibody in specificity and antigen-binding affinity (K_D = 45 nM). Consequently, the back mutation L49Y (tyrosine to histidine) led to the generation of HM1, which completely restored the binding ability of its murine counterpart.

4. 4 Potential clinical application in cancer therapy

Recently, humanized antibodies have been used in clinical trials for human cancer treatment (Qu et al., 2005). The original murine anti-EREG antibody 9E5 is potentially useful marker for the diagnosis of colon cancer since it is detected in tumor cells from transplanted mouse models (data not shown). However, this promise has not yet been realized largely because of the antibody's murine origin and the clinical application of murine 9E5 is limited by the HAMA response. In this study, I humanized the 9E5 murine antibody and the results of the incidence rate of antibodies (Section 3. 3) and Z-Score analyses (Section 4. 2. 3) suggest that the immunogenicity of the humanized anti-EREG antibodies was much lower than that of the original murine antibody. Because of the reduced immunogenicity and cancer cell-binding function of the humanized anti-EREG antibody, HM1 may have potential applications in clinical diagnosis.

In addition, the humanized anti-EREG antibodies contain a human IgG1 constant region that is effective for recruiting human immune effector function, including CDC and ADCC. Co et al. (Co et al., 1996) reported that a humanized IgG1 antibody could mediate tumor-killing activity in the presence of human effector cells (through ADCC) or human serum (through CDC), and Houghton et al (Houghton, 1983) also reported that partial tumor regression could be achieved by a humanized antibody possessing the effector function activities (CDC/ADCC). Thus, the humanized anti-EREG antibodies itself should have the potential to process the anti-cancer activity without the need to be conjugated with other toxic agents. Moreover, as an IgG1 molecule, the long serum half-life of humanized anti-EREG antibody allows it to be retained in the human body for a long period before being degraded. Thus, it could be a potential therapeutic

agent for EREG-positive cancers. In future, before performing clinical trials, the anti-cancer ability of the humanized anti-EREG needs to be addressed at the pre-clinical level.

4. 5 Conclusion

EREG, which is a tumor-specific antigen, is a ligand binding to the epidermal growth factor receptor and a protein whose expression increases in human colon cancer cell lines. When humanizing the therapeutic murine anti-EREG antibody, the key issue is to preserve their affinity and biological function simultaneously. In this study, I describe the construction and expression of humanized antibodies of 9E5, which will be used as a new approach to determine the key murine framework region residues that interact with the CDR to be substituted into the human acceptor framework to preserve the CDR conformations. Importantly, only one mutation in the frameworks was sufficient to recover the binding capability of a humanized antibody. In addition, the HM1 heavy and light chain frameworks showed humanness scores of 0.270 (heavy) and 0.092 (light), respectively. It suggested that the immunogenicity of the humanized anti-EREG antibodies was much lower than that of the original murine antibody. The reduced immunogenicity and cancer cell-binding function of the humanized anti-EREG antibody HM1 may have potential applications in clinical settings.

Moreover, this study support that HM1 contains a human IgG1 constant region that is effective for recruiting human immune effector function, including CDC and ADCC. All these results show that the humanized anti-EREG antibody is successfully expressed as an IgG1 complete antibody and that this humanized anti-EREG antibody can bind specifically to human colorectal carcinoma cells, thus possessing the potential for further development as a candidate

therapeutic and research tool. In future, in the next antibody design, I am also interested in improving the cancer cell-binding activity.

References

Abhinandan, K.R., and Martin, A.C.R. (2007). Analyzing the “Degree of Humanness” of Antibody Sequences. Journal of Molecular Biology *369*, 852–862.

Abrams, P. (1993). Have monoclonals fulfilled their promise? Nat Biotechnol *11*, 156–157.

Aggarwal, S. (2007). What's fueling the biotech engine? Nat Biotechnol *25*, 1097–1104.

Allcorn, L.C., and Martin, A.C.R. (2002). SACS—Self-maintaining database of antibody crystal structure information. Bioinformatics.

Avraham, R., and Yarden, Y. (2011). Feedback regulation of EGFR signalling: decision making by early and delayed loops. Nat Rev Mol Cell Biol *12*, 104–117.

Baba, I., Shirasawa, S., Iwamoto, R., Okumura, K., Tsunoda, T., Nishioka, M., Fukuyama, K., Yamamoto, K., Mekada, E., and Sasazuki, T. (2000). Involvement of deregulated epiregulin expression in tumorigenesis in vivo through activated Ki-Ras signaling pathway in human colon cancer cells. Cancer Research *60*, 6886–6889.

Barozzi, C., Ravaioli, M., D'Errico, A., and Grazi, G.L. (2002). Relevance of biologic markers in colorectal carcinoma. Cancer.

Bender, N.K., Heilig, C.E., Dröll, B., Wohlgemuth, J., Armbruster, F.-P., and Heilig, B. (2007). Immunogenicity, efficacy and adverse events of adalimumab in RA patients. Rheumatol. Int. *27*, 269–274.

Bennett, N.T., and Schultz, G.S. (1993). Growth factors and wound healing: Biochemical properties of growth factors and their receptors. The American Journal of Surgery *165*, 728–737.

Britten, C.D. (2004). Targeting ErbB receptor signaling: a pan-ErbB approach to cancer. Mol. Cancer Ther. *3*, 1335–1342.

Carpenter, G., and COHEN, S. (1990). Epidermal growth factor. J. Biol. Chem.

Carter, P. (2001). Improving the efficacy of antibody-based cancer therapies. Nat Rev Cancer *1*, 118–129.

Cartron, G., Dacheux, L., Salles, G., Solal-Celigny, P., Bardos, P., Colombat, P., and Watier, H. (2002). Therapeutic activity of humanized anti-CD20 monoclonal antibody and polymorphism in IgG Fc receptor FcgammaRIIIa gene. Blood *99*, 754–758.

Chan, A.C., and Carter, P.J. (2010). Therapeutic antibodies for autoimmunity and inflammation. Nat Rev Immunol *10*, 301–316.

Chothia, C., Lesk, A.M., Gherardi, E., Tomlinson, I.M., Walter, G., Marks, J.D., Llewelyn, M.B., and Winter, G. (1992). Structural repertoire of the human VH segments. Journal of Molecular Biology *227*, 799–817.

Ciardiello, F., and Tortora, G. (2008). EGFR antagonists in cancer treatment. N. Engl. J. Med. *358*, 1160–1174.

Co, M.S., Baker, J., Bednarik, K., Janzek, E., Neruda, W., Mayer, P., Plot, R., Stumper, B., Vasquez, M., Queen, C., et al. (1996). Humanized anti-Lewis Y antibodies: in vitro properties and pharmacokinetics in rhesus monkeys. Cancer Research *56*, 1118–1125.

COHEN, S. (1962). Isolation of a mouse submaxillary gland protein accelerating incisor eruption and eyelid opening in the new-born animal. J. Biol. Chem. *237*, 1555–1562.

Daub, H., Weiss, F.U., Wallasch, C., and Ullrich, A. (1996). Role of transactivation of the EGF receptor in signalling by G-protein-coupled receptors. Nature *379*, 557–560.

Engelman, J.A., Zejnullahu, K., Mitsudomi, T., Song, Y., Hyland, C., Park, J.O., Lindeman, N., Gale, C.-M., Zhao, X., Christensen, J., et al. (2007). MET amplification leads to gefitinib resistance in lung cancer by activating ERBB3 signaling. Science *316*, 1039–1043.

Fischer, O.M., Hart, S., Gschwind, A., and Ullrich, A. (2003). EGFR signal transactivation in cancer cells. Biochem. Soc. Trans. *31*, 1203–1208.

Foote, J., and Winter, G. (1992). Antibody framework residues affecting the conformation of the hypervariable loops. Journal of Molecular Biology *224*, 487–499.

Freimann, S., Ben-Ami, I., Hirsh, L., Dantes, A., Halperin, R., and Amsterdam, A. (2004). Drug development for ovarian hyper-stimulation and anti-cancer treatment: blocking of gonadotropin signaling for epiregulin and amphiregulin biosynthesis. Biochemical Pharmacology *68*, 989–996.

Geer, P.V., Hunter, T., and Lindberg, R.A. (1994). Receptor protein-tyrosine kinases and their signal transduction pathways. Annual Review of Cell Biology.

George, A.J. (1994). Antibody engineering. Endeavour *18*, 27–31.

Gram, H., Marconi, L.A., Barbas, C.F., Collet, T.A., Lerner, R.A., and Kang, A.S. (1992). In vitro selection and affinity maturation of antibodies from a naive combinatorial immunoglobulin library. Proc. Natl. Acad. Sci. U.S.a. *89*, 3576–3580.

Grandis, J.R., Chakraborty, A., and Zeng, Q. (1998). Downmodulation of TGF-α protein expression with antisense oligonucleotides inhibits proliferation of head and neck squamous carcinoma but not normal mucosal …. Journal of Cellular ….

Hanahan, D., Ono, Y., Sasada, R., Igarashi, K., and Folkman, J. (1993). Betacellulin: a mitogen from pancreatic beta cell tumors. Science.

Higashiyama, S., Abraham, J.A., Miller, J., Fiddes, J.C., and Klagsbrun, M. (1991). A heparin-binding growth factor secreted by macrophage-like cells that is related to EGF. Science *251*, 936–939.

Holbro, T. (2003). The ErbB receptors and their role in cancer progression. Experimental Cell Research *284*, 99–110.

Holmes, W.E., Sliwkowski, M.X., Akita, R.W., Henzel, W.J., Lee, J., Park, J.W., Yansura, D., Abadi, N., Raab, H., and Lewis, G.D. (1992). Identification of heregulin, a specific activator of p185erbB2. Science *256*, 1205–1210.

Houghton, A.N. (1983). Detection of cell surface and intracellular antigens by human monoclonal antibodies. Hybrid cell lines derived from lymphocytes of patients with malignant melanoma. Journal of Experimental Medicine *158*, 53–65.

Hurwitz, H., Fehrenbacher, L., Novotny, W., Cartwright, T., Hainsworth, J., Heim, W., Berlin, J., Baron, A., Griffing, S., Holmgren, E., et al. (2004). Bevacizumab plus irinotecan, fluorouracil, and leucovorin for metastatic colorectal cancer. N. Engl. J. Med. *350*, 2335–2342.

Hynes, N.E., and Lane, H.A. (2005). ERBB receptors and cancer: the complexity of targeted inhibitors. Nat Rev Cancer *5*, 341–354.

Jeffrey, P.D., Strong, R.K., Sieker, L.C., Chang, C.Y., Campbell, R.L., Petsko, G.A., Haber, E., Margolies, M.N., and Sheriff, S. (1993). 26-10 Fab-digoxin complex: affinity and specificity due to surface complementarity. Proc. Natl. Acad. Sci. U.S.a. *90*, 10310–10314.

Jemal, A., Bray, F., Center, M.M., Ferlay, J., Ward, E., and Forman, D. (2011). Global cancer statistics. CA: a Cancer Journal for Clinicians *61*, 69–90.

Jones, P.T., Dear, P.H., Foote, J., Neuberger, M.S., and Winter, G. (1986). Replacing the complementarity-determining regions in a human antibody with those from a mouse. Nature *321*, 522–525.

Kobayashi, S., Yamada-Okabe, H., Suzuki, M., Natori, O., Kato, A., Matsubara, K., Jau Chen, Y., Yamazaki, M., Funahashi, S., Yoshida, K., et al. (2012). LGR5-Positive Colon Cancer Stem Cells Interconvert with Drug-Resistant LGR5-Negative cells and are Capable of Tumor Reconstitution. Stem Cells *30*, 2631–2644.

Koren, E., Zuckerman, L.A., and Mire-Sluis, A.R. (2002). Immune responses to therapeutic proteins in humans--clinical significance, assessment and prediction. Curr Pharm Biotechnol *3*, 349–360.

Laskin, J.J., and Sandler, A.B. (2004). Epidermal growth factor receptor: a promising target in solid tumours. Cancer Treat. Rev. *30*, 1–17.

Lefranc, M.-P. (2004). IMGT-ONTOLOGY and IMGT databases, tools and Web resources for immunogenetics and immunoinformatics. Molecular Immunology *40*, 647–660.

Lu, H.S. (2001). Crystal Structure of Human Epidermal Growth Factor and Its Dimerization. Journal of Biological Chemistry *276*, 34913–34917.

Makabe, K., Nakanishi, T., Tsumoto, K., Tanaka, Y., Kondo, H., Umetsu, M., Sone, Y., Asano, R., and Kumagai, I. (2008). Thermodynamic Consequences of Mutations in Vernier Zone Residues of a Humanized Anti-human Epidermal Growth Factor Receptor Murine Antibody, 528. Journal of Biological Chemistry *283*, 1156–1166.

Marquardt, H., Hunkapiller, M.W., Hood, L.E., and Todaro, G.J. (1984). Rat transforming growth factor type 1: structure and relation to epidermal growth factor. Science *223*, 1079–1082.

Mazor, Y., Van Blarcom, T., Mabry, R., Iverson, B.L., and Georgiou, G. (2007). Isolation of engineered, full-length antibodies from libraries expressed in Escherichia coli. Nat Biotechnol *25*, 563–565.

Mian, I.S., Bradwell, A.R., and Olson, A.J. (1991). Structure, function and properties of antibody binding sites. Journal of Molecular Biology *217*, 133–151.

Nimmerjahn, F., and Ravetch, J.V. (2006). Fcγ Receptors: Old Friends and New Family Members. Immunity *24*, 19–28.

Nimmerjahn, F., and Ravetch, J.V. (2008). Fcgamma receptors as regulators of immune responses. Nat Rev Immunol *8*, 34–47.

Ogiso, H., Ishitani, R., Nureki, O., Fukai, S., Yamanaka, M., Kim, J.-H., Saito, K., Sakamoto, A., Inoue, M., Shirouzu, M., et al. (2002). Crystal structure of the complex of human epidermal growth factor and receptor extracellular domains. Cell *110*, 775–787.

Okines, A., Cunningham, D., and Chau, I. (2011). Targeting the human EGFR family in esophagogastric cancer. Nat Rev Clin Oncol *8*, 492–503.

Padlan, E.A. (1994). Anatomy of the antibody molecule. Molecular Immunology *31*, 169–217.

Pedersen, J.T., Henry, A.H., Searle, S.J., Guild, B.C., Roguska, M., and Rees, A.R. (1994). Comparison of surface accessible residues in human and murine immunoglobulin Fv domains. Implication for humanization of murine antibodies. Journal of Molecular Biology *235*, 959–973.

Pettersen, E.F., Goddard, T.D., Huang, C.C., Couch, G.S., Greenblatt, D.M., Meng, E.C., and Ferrin, T.E. (2004). UCSF Chimera?A visualization system for exploratory research and analysis. J. Comput. Chem. *25*, 1605–1612.

Presta, L.G., Lahr, S.J., Shields, R.L., Porter, J.P., Gorman, C.M., Fendly, B.M., and Jardieu, P.M. (1993). Humanization of an antibody directed against IgE. J. Immunol. *151*, 2623–2632.

Pusztai, L., Lewis, C.E., Lorenzen, J., and McGee, J.O. (1993). Growth factors: Regulation of normal and neoplastic growth. J. Pathol. *169*, 191–201.

Qu, Z., Griffiths, G.L., Wegener, W.A., Chang, C.-H., Govindan, S.V., Horak, I.D., Hansen, H.J., and Goldenberg, D.M. (2005). Development of humanized antibodies as cancer therapeutics. Methods *36*, 84–95.

Ravetch, J.V., Clynes, R.A., Towers, T.L., and Presta, L.G. (2000). Inhibitory Fc receptors modulate in vivo cytoxicity against tumor targets - Nature Medicine. Nat. Med. *6*, 443–446.

Reichert, J.M. (2010). Antibodies to watch in 2010. Mabs *2*, 84–100.

Reichert, J.M., Rosensweig, C.J., Faden, L.B., and Dewitz, M.C. (2005). Monoclonal antibody successes in the clinic. Nat Biotechnol *23*, 1073–1078.

Revillion, F., Lhotellier, V., Hornez, L., Bonneterre, J., and Peyrat, J.P. (2007). ErbB/HER ligands in human breast cancer, and relationships with their receptors, the bio-pathological features and prognosis. Annals of Oncology *19*, 73–80.

Riechmann, L., Clark, M., Waldmann, H., and Winter, G. (1988). Reshaping human antibodies for therapy. Nature *332*, 323–327.

Ritter, C.A., Perez-Torres, M., Rinehart, C., Guix, M., Dugger, T., Engelman, J.A., and Arteaga, C.L. (2007). Human breast cancer cells selected for resistance to trastuzumab in vivo overexpress epidermal growth factor receptor and ErbB ligands and remain dependent on the ErbB receptor network. Clin. Cancer Res. *13*, 4909–4919.

Salomon, D.S., Brandt, R., Ciardiello, F., and Normanno, N. (1995). Epidermal growth factor-related peptides and their receptors in human malignancies. Crit. Rev. Oncol. Hematol. *19*, 183–232.

Sasada, R., Onda, H., and Igarashi, K. (1987). The establishment of IL-2 producing cells by genetic engineering. Cell Structure and Function *12*, 205.

Scott, A.M., Wolchok, J.D., and Old, L.J. (2012). Antibody therapy of cancer. Nat Rev Cancer *12*, 278–287.

Shoyab, M., Plowman, G.D., McDonald, V.L., Bradley, J.G., and Todaro, G.J. (1989). Structure and function of human amphiregulin: a member of the epidermal growth factor family. Science *243*, 1074–1076.

Sircar, A., Kim, E.T., and Gray, J.J. (2009). RosettaAntibody: antibody variable region homology modeling server. Nucleic Acids Research *37*, W474–W479.

Sivasubramanian, A., Sircar, A., Chaudhury, S., and Gray, J.J. (2009). Toward high-resolution homology modeling of antibody Fv regions and application to antibody-antigen docking. Proteins *74*, 497–514.

Tannock, I.F., and Rotin, D. (1989). Acid pH in tumors and its potential for therapeutic exploitation. Cancer Research *49*, 4373–4384.

Thøgersen, V.B., Sørensen, B.S., Poulsen, S.S., Orntoft, T.F., Wolf, H., and Nexo, E. (2001). A subclass of HER1 ligands are prognostic markers for survival in bladder cancer patients. Cancer Research *61*, 6227–6233.

Toyoda, H., Komurasaki, T., Uchida, D., and Morimoto, S. (1997). Distribution of mRNA for human epiregulin, a differentially expressed member of the epidermal growth factor family. Biochem. J. *326 (Pt 1)*, 69–75.

Toyoda, H., Komurasaki, T., Uchida, D., Takayama, Y., Isobe, T., Okuyama, T., and Hanada, K. (1995). Epiregulin A novel epidermal growth factor with mitogenic activity for rat primary hepatocytes. J. Biol. Chem. *270*, 7495–7500.

Trutnau, H.H. (2006). New multi-step kinetics using common affinity biosensors saves time and sample at full access to kinetics and concentration. Journal of Biotechnology *124*, 191–195.

Tørring, N., Hansen, F.D., Sørensen, B.S., Ørntoft, T.F., and Nexø, E. (2005). Increase in amphiregulin and epiregulin in prostate cancer xenograft after androgen deprivation—impact of specific HER1 inhibition. Prostate *64*, 1–8.

Valabrega, G., Montemurro, F., Sarotto, I., Petrelli, A., Rubini, P., Tacchetti, C., Aglietta, M., Comoglio, P.M., and Giordano, S. (2005). TGFalpha expression impairs Trastuzumab-induced HER2 downregulation. Oncogene *24*, 3002–3010.

Wang, F., Liu, R., Lee, S.W., Sloss, C.M., Couget, J., and Cusack, J.C. (2007). Heparin-binding EGF-like growth factor is an early response gene to chemotherapy and contributes to chemotherapy resistance. Oncogene *26*, 2006–2016.

Weiner, L.M., Surana, R., and Wang, S. (2010). Monoclonal antibodies: versatile platforms for cancer immunotherapy. Nat Rev Immunol *10*, 317–327.

Wen, D., Peles, E., Cupples, R., Suggs, S.V., Bacus, S.S., Luo, Y., Trail, G., Hu, S., Silbiger, S.M., and Levy, R.B. (1992). Neu differentiation factor: a transmembrane glycoprotein containing an EGF domain and an immunoglobulin homology unit. Cell *69*, 559–572.

Winter, G., and Harris, W.J. (1993). Humanized antibodies. Trends in Pharmacological Sciences *14*, 139–143.

Yarden, Y., and Sliwkowski, M.X. (2001). Untangling the ErbB signalling network. Nat Rev Mol Cell Biol *2*, 127–137.

Yun, J., Song, S.-H., Park, J., Kim, H.-P., Yoon, Y.-K., Lee, K.-H., Han, S.-W., Oh, D.-Y., Im, S.-A., Bang, Y.-J., et al. (2012). Gene silencing of EREG mediated by DNA methylation and histone modification in human gastric cancers. Lab. Invest. *92*, 1033–1044.

Abhinandan, K.R., and Martin, A.C.R. (2007). Analyzing the “Degree of Humanness” of Antibody Sequences. Journal of Molecular Biology *369*, 852–862.

Abrams, P. (1993). Have monoclonals fulfilled their promise? Nat Biotechnol *11*, 156–157.

Aggarwal, S. (2007). What's fueling the biotech engine? Nat Biotechnol *25*, 1097–1104.

Allcorn, L.C., and Martin, A.C.R. (2002). SACS—Self-maintaining database of antibody crystal structure information. Bioinformatics.

Avraham, R., and Yarden, Y. (2011). Feedback regulation of EGFR signalling: decision making by early and delayed loops. Nat Rev Mol Cell Biol *12*, 104–117.

Baba, I., Shirasawa, S., Iwamoto, R., Okumura, K., Tsunoda, T., Nishioka, M., Fukuyama, K., Yamamoto, K., Mekada, E., and Sasazuki, T. (2000). Involvement of deregulated epiregulin expression in tumorigenesis in vivo through activated Ki-Ras signaling pathway in human colon cancer cells. Cancer Research *60*, 6886–6889.

Barozzi, C., Ravaioli, M., D'Errico, A., and Grazi, G.L. (2002). Relevance of biologic markers in colorectal carcinoma. Cancer.

Bender, N.K., Heilig, C.E., Dröll, B., Wohlgemuth, J., Armbruster, F.-P., and Heilig, B. (2007). Immunogenicity, efficacy and adverse events of adalimumab in RA patients. Rheumatol. Int. *27*, 269–274.

Bennett, N.T., and Schultz, G.S. (1993). Growth factors and wound healing: Biochemical properties of growth factors and their receptors. The American Journal of Surgery *165*, 728–737.

Britten, C.D. (2004). Targeting ErbB receptor signaling: a pan-ErbB approach to cancer. Mol. Cancer Ther. *3*, 1335–1342.

Carpenter, G., and COHEN, S. (1990). Epidermal growth factor. J. Biol. Chem.

Carter, P. (2001). Improving the efficacy of antibody-based cancer therapies. Nat Rev Cancer *1*, 118–129.

Cartron, G., Dacheux, L., Salles, G., Solal-Celigny, P., Bardos, P., Colombat, P., and Watier, H. (2002). Therapeutic activity of humanized anti-CD20 monoclonal antibody and polymorphism in IgG Fc receptor FcgammaRIIIa gene. Blood *99*, 754–758.

Chan, A.C., and Carter, P.J. (2010). Therapeutic antibodies for autoimmunity and inflammation. Nat Rev Immunol *10*, 301–316.

Chothia, C., Lesk, A.M., Gherardi, E., Tomlinson, I.M., Walter, G., Marks, J.D., Llewelyn, M.B., and Winter, G. (1992). Structural repertoire of the human VH segments. Journal of Molecular Biology *227*, 799–817.

Ciardiello, F., and Tortora, G. (2008). EGFR antagonists in cancer treatment. N. Engl. J. Med. *358*, 1160–1174.

Co, M.S., Baker, J., Bednarik, K., Janzek, E., Neruda, W., Mayer, P., Plot, R., Stumper, B., Vasquez, M., Queen, C., et al. (1996). Humanized anti-Lewis Y antibodies: in vitro properties and pharmacokinetics in rhesus monkeys. Cancer Research *56*, 1118–1125.

COHEN, S. (1962). Isolation of a mouse submaxillary gland protein accelerating incisor eruption and eyelid opening in the new-born animal. J. Biol. Chem. *237*, 1555–1562.

Daub, H., Weiss, F.U., Wallasch, C., and Ullrich, A. (1996). Role of transactivation of the EGF receptor in signalling by G-protein-coupled receptors. Nature *379*, 557–560.

Engelman, J.A., Zejnullahu, K., Mitsudomi, T., Song, Y., Hyland, C., Park, J.O., Lindeman, N., Gale, C.-M., Zhao, X., Christensen, J., et al. (2007). MET amplification leads to gefitinib resistance in lung cancer by activating ERBB3 signaling. Science *316*, 1039–1043.

Fischer, O.M., Hart, S., Gschwind, A., and Ullrich, A. (2003). EGFR signal transactivation in cancer cells. Biochem. Soc. Trans. *31*, 1203–1208.

Foote, J., and Winter, G. (1992). Antibody framework residues affecting the conformation of the hypervariable loops. Journal of Molecular Biology *224*, 487–499.

Freimann, S., Ben-Ami, I., Hirsh, L., Dantes, A., Halperin, R., and Amsterdam, A. (2004). Drug development for ovarian hyper-stimulation and anti-cancer treatment: blocking of gonadotropin signaling for epiregulin and amphiregulin biosynthesis. Biochemical Pharmacology *68*, 989–996.

George, A.J. (1994). Antibody engineering. Endeavour *18*, 27–31.

Gram, H., Marconi, L.A., Barbas, C.F., Collet, T.A., Lerner, R.A., and Kang, A.S. (1992). In vitro selection and affinity maturation of antibodies from a naive combinatorial immunoglobulin library. Proc. Natl. Acad. Sci. U.S.a. *89*, 3576–3580.

Grandis, J.R., Chakraborty, A., and Zeng, Q. (1998). Downmodulation of TGF-α protein expression with antisense oligonucleotides inhibits proliferation of head and neck squamous carcinoma but not normal mucosal …. Journal of Cellular ….

Hanahan, D., Ono, Y., Sasada, R., Igarashi, K., and Folkman, J. (1993). Betacellulin: a mitogen from pancreatic beta cell tumors. Science.

Higashiyama, S., Abraham, J.A., Miller, J., Fiddes, J.C., and Klagsbrun, M. (1991). A heparin-binding growth factor secreted by macrophage-like cells that is related to EGF. Science *251*, 936–939.

Holbro, T. (2003). The ErbB receptors and their role in cancer progression. Experimental Cell Research *284*, 99–110.

Holmes, W.E., Sliwkowski, M.X., Akita, R.W., Henzel, W.J., Lee, J., Park, J.W., Yansura, D., Abadi, N., Raab, H., and Lewis, G.D. (1992). Identification of heregulin, a specific activator of p185erbB2. Science *256*, 1205–1210.

Houghton, A.N. (1983). Detection of cell surface and intracellular antigens by human monoclonal antibodies. Hybrid cell lines derived from lymphocytes of patients with malignant melanoma. Journal of Experimental Medicine *158*, 53–65.

Hurwitz, H., Fehrenbacher, L., Novotny, W., Cartwright, T., Hainsworth, J., Heim, W., Berlin, J., Baron, A., Griffing, S., Holmgren, E., et al. (2004). Bevacizumab plus irinotecan, fluorouracil, and leucovorin for metastatic colorectal cancer. N. Engl. J. Med. *350*, 2335–2342.

Hynes, N.E., and Lane, H.A. (2005). ERBB receptors and cancer: the complexity of targeted inhibitors. Nat Rev Cancer *5*, 341–354.

Jeffrey, P.D., Strong, R.K., Sieker, L.C., Chang, C.Y., Campbell, R.L., Petsko, G.A., Haber, E., Margolies, M.N., and Sheriff, S. (1993). 26-10 Fab-digoxin complex: affinity and specificity due to surface complementarity. Proc. Natl. Acad. Sci. U.S.a. *90*, 10310–10314.

Jemal, A., Bray, F., Center, M.M., Ferlay, J., Ward, E., and Forman, D. (2011). Global cancer statistics. CA: a Cancer Journal for Clinicians *61*, 69–90.

Jones, P.T., Dear, P.H., Foote, J., Neuberger, M.S., and Winter, G. (1986). Replacing the complementarity-determining regions in a human antibody with those from a mouse. Nature *321*, 522–525.

Kobayashi, S., Yamada-Okabe, H., Suzuki, M., Natori, O., Kato, A., Matsubara, K., Jau Chen, Y., Yamazaki, M., Funahashi, S., Yoshida, K., et al. (2012). LGR5-Positive Colon Cancer Stem Cells Interconvert with Drug-Resistant LGR5-Negative cells and are Capable of Tumor Reconstitution. Stem Cells *30*, 2631–2644.

Koren, E., Zuckerman, L.A., and Mire-Sluis, A.R. (2002). Immune responses to therapeutic proteins in humans--clinical significance, assessment and prediction. Curr Pharm Biotechnol *3*, 349–360.

Laskin, J.J., and Sandler, A.B. (2004). Epidermal growth factor receptor: a promising target in solid tumours. Cancer Treat. Rev. *30*, 1–17.

Lefranc, M.-P. (2004). IMGT-ONTOLOGY and IMGT databases, tools and Web resources for immunogenetics and immunoinformatics. Molecular Immunology *40*, 647–660.

Lu, H.S. (2001). Crystal Structure of Human Epidermal Growth Factor and Its Dimerization. Journal of Biological Chemistry *276*, 34913–34917.

Makabe, K., Nakanishi, T., Tsumoto, K., Tanaka, Y., Kondo, H., Umetsu, M., Sone, Y., Asano, R., and Kumagai, I. (2008). Thermodynamic Consequences of Mutations in Vernier Zone Residues of a Humanized Anti-human Epidermal Growth Factor Receptor Murine Antibody, 528. Journal of Biological Chemistry *283*, 1156–1166.

Marquardt, H., Hunkapiller, M.W., Hood, L.E., and Todaro, G.J. (1984). Rat transforming growth factor type 1: structure and relation to epidermal growth factor. Science *223*, 1079–1082.

Mazor, Y., Van Blarcom, T., Mabry, R., Iverson, B.L., and Georgiou, G. (2007). Isolation of engineered, full-length antibodies from libraries expressed in Escherichia coli. Nat Biotechnol *25*, 563–565.

Mian, I.S., Bradwell, A.R., and Olson, A.J. (1991). Structure, function and properties of antibody binding sites. Journal of Molecular Biology *217*, 133–151.

Nimmerjahn, F., and Ravetch, J.V. (2006). Fcγ Receptors: Old Friends and New Family Members. Immunity *24*, 19–28.

Nimmerjahn, F., and Ravetch, J.V. (2008). Fcgamma receptors as regulators of immune responses. Nat Rev Immunol *8*, 34–47.

Ogiso, H., Ishitani, R., Nureki, O., Fukai, S., Yamanaka, M., Kim, J.-H., Saito, K., Sakamoto, A., Inoue, M., Shirouzu, M., et al. (2002). Crystal structure of the complex of human epidermal growth factor and receptor extracellular domains. Cell *110*, 775–787.

Padlan, E.A. (1994). Anatomy of the antibody molecule. Molecular Immunology *31*, 169–217.

Pedersen, J.T., Henry, A.H., Searle, S.J., Guild, B.C., Roguska, M., and Rees, A.R. (1994). Comparison of surface accessible residues in human and murine immunoglobulin Fv domains. Implication for humanization of murine antibodies. Journal of Molecular Biology *235*, 959–973.

Pettersen, E.F., Goddard, T.D., Huang, C.C., Couch, G.S., Greenblatt, D.M., Meng, E.C., and Ferrin, T.E. (2004). UCSF Chimera?A visualization system for exploratory research and analysis. J. Comput. Chem. *25*, 1605–1612.

Presta, L.G., Lahr, S.J., Shields, R.L., Porter, J.P., Gorman, C.M., Fendly, B.M., and Jardieu, P.M. (1993). Humanization of an antibody directed against IgE. J. Immunol. *151*, 2623–2632.

Pusztai, L., Lewis, C.E., Lorenzen, J., and McGee, J.O. (1993). Growth factors: Regulation of normal and neoplastic growth. J. Pathol. *169*, 191–201.

Qu, Z., Griffiths, G.L., Wegener, W.A., Chang, C.-H., Govindan, S.V., Horak, I.D., Hansen, H.J., and Goldenberg, D.M. (2005). Development of humanized antibodies as cancer therapeutics. Methods *36*, 84–95.

Ravetch, J.V., Clynes, R.A., Towers, T.L., and Presta, L.G. (2000). Inhibitory Fc receptors modulate in vivo cytoxicity against tumor targets - Nature Medicine. Nat. Med. *6*, 443–446.

Reichert, J.M. (2010). Antibodies to watch in 2010. Mabs *2*, 84–100.

Reichert, J.M., Rosensweig, C.J., Faden, L.B., and Dewitz, M.C. (2005). Monoclonal antibody successes in the clinic. Nat Biotechnol *23*, 1073–1078.

Revillion, F., Lhotellier, V., Hornez, L., Bonneterre, J., and Peyrat, J.P. (2007). ErbB/HER ligands in human breast cancer, and relationships with their receptors, the bio-pathological features and prognosis. Annals of Oncology *19*, 73–80.

Riechmann, L., Clark, M., Waldmann, H., and Winter, G. (1988). Reshaping human antibodies for therapy. Nature *332*, 323–327.

Ritter, C.A., Perez-Torres, M., Rinehart, C., Guix, M., Dugger, T., Engelman, J.A., and Arteaga, C.L. (2007). Human breast cancer cells selected for resistance to trastuzumab in vivo overexpress epidermal growth factor receptor and ErbB ligands and remain dependent on the ErbB receptor network. Clin. Cancer Res. *13*, 4909–4919.

Roguska, M.A., Pedersen, J.T., Henry, A.H., Searle, S.M., Roja, C.M., Avery, B., Hoffee, M., Cook, S., Lambert, J.M., Blättler, W.A., et al. (1996). A comparison of two murine monoclonal antibodies humanized by CDR-grafting and variable domain resurfacing. Protein Eng. *9*, 895–904.

Rush, J.S., Quinalty, L.M., Engelman, L., Sherry, D.M., and Ceresa, B.P. (2012). Endosomal accumulation of the activated epidermal growth factor receptor (EGFR) induces apoptosis. J. Biol. Chem. *287*, 712–722.

Salomon, D.S., Brandt, R., Ciardiello, F., and Normanno, N. (1995). Epidermal growth factor-related peptides and their receptors in human malignancies. Crit. Rev. Oncol. Hematol. *19*, 183–232.

Sasada, R., Onda, H., and Igarashi, K. (1987). The establishment of IL-2 producing cells by genetic engineering. Cell Structure and Function *12*, 205.

Scott, A.M., Wolchok, J.D., and Old, L.J. (2012). Antibody therapy of cancer. Nat Rev Cancer *12*, 278–287.

Shoyab, M., Plowman, G.D., McDonald, V.L., Bradley, J.G., and Todaro, G.J. (1989). Structure and function of human amphiregulin: a member of the epidermal growth factor family. Science *243*, 1074–1076.

Sircar, A., Kim, E.T., and Gray, J.J. (2009). RosettaAntibody: antibody variable region homology modeling server. Nucleic Acids Research *37*, W474–W479.

Sivasubramanian, A., Sircar, A., Chaudhury, S., and Gray, J.J. (2009). Toward high-resolution homology modeling of antibody Fv regions and application to antibody-antigen docking. Proteins *74*, 497–514.

Tannock, I.F., and Rotin, D. (1989). Acid pH in tumors and its potential for therapeutic exploitation. Cancer Research *49*, 4373–4384.

Teng, G., and Papavasiliou, F.N. (2007). Immunoglobulin Somatic Hypermutation. Annu. Rev. Genet. *41*, 107–120.

Thøgersen, V.B., Sørensen, B.S., Poulsen, S.S., Orntoft, T.F., Wolf, H., and Nexo, E. (2001). A subclass of HER1 ligands are prognostic markers for survival in bladder cancer patients. Cancer Research *61*, 6227–6233.

Toyoda, H., Komurasaki, T., Uchida, D., and Morimoto, S. (1997). Distribution of mRNA for human epiregulin, a differentially expressed member of the epidermal growth factor family. Biochem. J. *326 (Pt 1)*, 69–75.

Toyoda, H., Komurasaki, T., Uchida, D., Takayama, Y., Isobe, T., Okuyama, T., and Hanada, K. (1995). Epiregulin A novel epidermal growth factor with mitogenic activity for rat primary hepatocytes. J. Biol. Chem. *270*, 7495–7500.

Trutnau, H.H. (2006). New multi-step kinetics using common affinity biosensors saves time and sample at full access to kinetics and concentration. Journal of Biotechnology *124*, 191–195.

Tørring, N., Hansen, F.D., Sørensen, B.S., Ørntoft, T.F., and Nexø, E. (2005). Increase in amphiregulin and epiregulin in prostate cancer xenograft after androgen deprivation—impact of specific HER1 inhibition. Prostate *64*, 1–8.

Valabrega, G., Montemurro, F., Sarotto, I., Petrelli, A., Rubini, P., Tacchetti, C., Aglietta, M., Comoglio, P.M., and Giordano, S. (2005). TGFalpha expression impairs Trastuzumab-induced HER2 downregulation. Oncogene *24*, 3002–3010.

Wang, F., Liu, R., Lee, S.W., Sloss, C.M., Couget, J., and Cusack, J.C. (2007). Heparin-binding EGF-like growth factor is an early response gene to chemotherapy and contributes to chemotherapy resistance. Oncogene *26*, 2006–2016.

Weiner, L.M., Surana, R., and Wang, S. (2010). Monoclonal antibodies: versatile platforms for cancer immunotherapy. Nat Rev Immunol *10*, 317–327.

Wen, D., Peles, E., Cupples, R., Suggs, S.V., Bacus, S.S., Luo, Y., Trail, G., Hu, S., Silbiger, S.M., and Levy, R.B. (1992). Neu differentiation factor: a transmembrane glycoprotein containing an EGF domain and an immunoglobulin homology unit. Cell *69*, 559–572.

Winter, G., and Harris, W.J. (1993). Humanized antibodies. Trends in Pharmacological Sciences *14*, 139–143.

Yarden, Y., and Sliwkowski, M.X. (2001). Untangling the ErbB signalling network. Nat Rev Mol Cell Biol *2*, 127–137.

Yun, J., Song, S.-H., Park, J., Kim, H.-P., Yoon, Y.-K., Lee, K.-H., Han, S.-W., Oh, D.-Y., Im, S.-A., Bang, Y.-J., et al. (2012). Gene silencing of EREG mediated by DNA methylation and histone modification in human gastric cancers. Lab. Invest. *92*, 1033–1044.

Appedix A1

< Primer used for amplification of VH>		
Name	Sequences	Tm(℃) & GC
h9E5-VH-p1	5- GGGTCAACTGGCGAT CAGGTTCAGCTGCAGC -3	Tm: 54, GC: 62%
h9E5-VH-p2	5- GGGTCAACTGGCGAT CAGGTTCAGCTGCAGC -3	Tm: 53, GC: 53%
CET1019 HD-Not1-SS-p1	5- TCCACGTGAGCCCGG ATGGAAACCGATACACTG -3	Tm: 50, GC: 44%
CET1019 HD-Not1-CH-p4	5- TCTTCGAATGCCCGG TCATCA TCATTTACCCGGAGACA -3	Tm: 50, GC: 47%
CET1019 HS-Nhe1-CH-p6	5- TCGAATGCGCGGATC TCA TCATTTACCCGGAGACA -3	Tm: 50, GC: 47%
h9E5IgGm1-VH-p1	5- ACGGCCGGCCGCTAG C ATGGAAACCGATACACTGC -3	Tm: 55, GC: 50%
h9E5IgGm1-VH-p2	5- TCGCGATCGCGCTAG C TCATTTACCCGGAGACAGG -3	Tm: 55, GC: 50%
CET1019HD-insert-p1	5- CTAGCGCGATCGCGA -3	Tm: 55, GC: 67%
< Primer used for amplification of VL >		
Name	Sequences	Tm(℃) & GC
h9E5-VL-p1	5- GGGTCAACTGGCGAT GACATCCAGATGACCCAGT -3	Tm: 55, GC: 53%
h9E5-VL-p2	5- TGCAGCCACCGTACG GGTACGTTTGATTTCAACTT -3	Tm: 50, GC: 35%
CET1019 HD-Nhe1-SS-p1	5- ACGGCCGGCCGGATC ATGGAAACCGATACACTG -3	Tm: 50, GC: 44%
CET1019 HD-Nhe1-CL-p4	5- TCGCGATCGCGGATC TCATCA ACACTCTCCCCTGTTG -3	Tm: 51, GC: 56%
CET1019 HS-Nhe1-CL-p6	5- TCGAATGCGCGGATC TCATCA ACACTCTCCCCTGTTG -3	Tm: 51, GC: 56%
h9E5IgGm1-VL-p1	5- TCCACGTGAGCGGCC GC ATGGAAACCGATACACTGC -3	Tm: 55, GC : 50%
h9E5IgGm1-VL-p2	5- TCTTCGAATGCGGCC GC TCAACACTCTCCCCTGTTG -3	Tm: 55, GC : 53%
CET1019HD-insert-p2	5- GGCCGCTCACGTG -3	Tm: 52, GC : 77%

Appedix A2

	One / Three letter code		Amino acid		Property	Size	One / Three letter code		Amino acid	Charge variation	Property	Size
Heavy chain												
EH1Q	E	Glu	Glutamic acid	H1	Charged : negative	big	Q	Gln	Glutamine	O	acidic / amide	big
LH11V	L	Leu	Leucine	H11	hydrophobic	big	V	Val	Valine		hydrophobic	small
VH12K	V	Val	Valine	H12	hydrophobic	small	K	Lys	Lysine	O	Charged : positive	big
LH20V	L	Leu	Leucine	H20	hydrophobic	big	V	Val	Valine		hydrophobic	small
TH23K	T	Thr	Threonine	H23	polar	small	K	Lys	Lysine	O	Charged : positive	big
KH38R	K	Lys	Lysine	H38	Charged : positive	big	R	Arg	Arginine		Charged : positive	
RH40A	R	Arg	Arginine	H40	Charged : positive		A	Ala	Alanine	O	polar	small
IH48M	I	Ile	Isoleucine	H48	hydrophobic	big	M	Met	Methionine		hydrophobic	big
KH67R	K	Lys	Lysine	H67	Charged : positive	big	R	Arg	Arginine		Charged : positive	
AH68V	A	Ala	Alanine	H68	polar	small	V	Val	Valine		hydrophobic	small
SH76T	S	Ser	Serine	H76	polar	small	T	Thr	Threonine		polar	small
SH78T	S	Ser	Serine	H78	polar	small	T	Thr	Threonine		polar	small
QH82E	Q	Gln	Glutamine	H82	acidic / amide	big	E	Glu	Glutamic acid	O	Charged : negative	big
SH97A	S	Ser	Serine	H97	polar	small	A	Ala	Alanine		polar	small
Light Chain												
LL15V	L	Leu	Leucine	L15	hydrophobic	big	V	Val	Valine		hydrophobic	small
GL17D	G	Gly	Glycine	L17	polar	small	D	Asp	Aspartic acid	O	acidic / amide	small
KL18R	K	Lys	Lysine	L18	Charged : positive	big	R	Arg	Arginine		Charged : positive	
IL33L	I	Ile	Isoleucine	L33	hydrophobic	big	L	Leu	Leucine		hydrophobic	big
KL42Q	K	Lys	Lysine	L42	Charged : positive	big	Q	Gln	Glutamine	O	acidic / amide	big
GL43A	G	Gly	Glycine	L43	polar	small	A	Ala	Alanine		polar	small
HL49Y	H	His	Histidine	L49	aromatic	big	Y	Tyr	Tyrosine	O	aromatic	big
RL69T	R	Arg	Arginine	L69	Charged : positive		T	Thr	Threonine	O	polar	small
YL71F	Y	Tyr	Tyrosine	L71	aromatic	big	F	Phe	Phenylalanine		aromatic	big
SL72T	S	Ser	Serine	L72	polar	small	T	Thr	Threonine		polar	small
NL77S	N	Asn	Asparagine	L77	acidic / amide	small	S	Ser	Serine		polar	small
EL79Q	E	Glu	Glutamic acid	L79	Charged : negative	big	Q	Gln	Glutamine	O	acidic / amide	big
LL103V	L	Leu	Leucine	L103	hydrophobic	big	V	Val	Valine		hydrophobic	small

Acknowledgements

I am most grateful to Prof. Akira Suyama for supervising my doctoral dissertation. I would like to thank Prof. Tatsuhiko Kodama, Prof. Yoshikazu Shibasaki, and Prof. Hirofumi Doi for helpful discussion and technical instructions. Finally, I thank a lot Kodama laboratory members and Shibasaki laboratory members, especially Dr. Mariko Iijima, Dr. Akira Sugiyama and Mr. Masazumi Ishii for their help.

This work was supported in part by Creation of Innovation Centers for Advanced Interdiciplinary Research Areas Program, Ministry of Education, Culture, Sports, Science and Technology-Japan.